Screening of anti-chronic nonbacterial prostatitis activity of different extractions of the aerial part of *Glycyrrhiza uralensis*, and network pharmacology research

HAIFAN LIU[1], JIE CUI[1], LIN ZHANG[2], GUANHUA CHANG[2] and WENQUAN WANG[1,3]

[1]Chinese Academy of Medical Sciences and Peking Union Medical College Institute of Medicinal Plant Development, Beijing 100193; [2]Beijing University of Chinese Medicine, Beijing 102488; [3]Engineering Research Center of Good Agricultural Practice for Chinese Crude Drugs, Ministry of Education, Beijing 100102, P.R. China

Received April 20, 2021; Accepted August 23, 2021

DOI: 10.3892/br.2021.1475

Abstract. In the present study, anti-chronic nonbacterial prostatitis (CNP) pharmacological experiments using water and ethanol extraction of the aerial parts of *Glycyrrhiza uralensis* were performed to select the best active parts by comparing their efficacy in a CNP model established by injecting carrageenin into the ventral lobe of rat prostate. The anti-CNP activities and expression of serum inflammatory factors in rats were also analyzed. A Protein-Protein Interaction network was constructed, and core targets were screened using topology and analyzed using Gene Ontology and Kyoto Encyclopedia of Genes and Genomes. Water and ethanol extraction exhibited good inhibitory effect on the pathological changes of the prostate tissue, the expression of inflammatory factors and fibrosis factors in CNP rats, whereas no differences were observed compared with the positive control drug. Water extraction was more effective and significantly reduced PGE2 expression ($P<0.05$). Network pharmacology assays showed 15 active components in the aerial part of *Glycyrrhiza uralensis*, and 9 key CNP therapeutic targets of the aerial parts of *Glycyrrhiza uralensis* were identified. The effect of water exraction on chronic prostatitis rats was significant. The aerial part of *Glycyrrhiza uralensis* down-regulated the levels of inflammatory factors and inhibited proinflammatory gene transcription, reduced oxidative stress response, inhibited cell survival pathways, regulated sex hormone levels, prevented immunostimulation and attenuated inflammation. This study provides a theoretical reference for the development of anti-CNP agents, and offers a novel methodology for identifying and clarifying the mechanisms underlying the efficacy of the anti-CNP components in the aerial part of *Glycyrrhiza uralensis*.

Correspondence to: Mrs. Jie Cui, Chinese Academy of Medical Sciences and Peking Union Medical College Institute of Medicinal Plant Development, 151 Malianwa North Road, Haidian, Beijing 100193, P.R. China
E-mail: 583486833@qq.com

Abbreviations: BP, biological process; CC, cellular component; CNP, chronic nonbacterial prostatitis; ER, estrogen receptor; GO, Gene Ontology; KEGG, Kyoto Encyclopedia of Genes and Genomes; MDC, macrophage-derived chemokine; MF, molecular function; PPI, Protein-Protein Interaction; ROS, reactive oxygen species; SD, Sprague-Dawley; TCM, Traditional Chinese medicine

Key words: aerial part of *Glycyrrhiza uralensis*, CNP, different extraction and enrichment parts, pharmacological experiment, active parts of efficacy, network pharmacology

Introduction

Glycyrrhiza uralensis, also known as Guolao, Lingtong, Sweet grass and Lolium, is the dried root and rhizome of *Glycyrrhiza uralensis Fisch*., *Glycyrrhiza inflata Bat* or *Glycyrrhiza glabra L*. *Glycyrrhiza uralensis*, and is traditionally used as a root and a rhizome. However, its aerial parts account for over one-third of the plant (1). Proper shoot trimming promotes the accumulation of active substances in the roots and rhizomes (2). A total of 61 flavonoids and 7 phenolic components have been isolated from the aerial part of *Glycyrrhiza uralensis* (3). Flavonoids possess antitumor, anti-AIDS, anti-ulcer, anti-inflammatory, anti-aging and other beneficial pharmacological properties (4). A total of 23 flavonoids have been identified by Bo *et al*, Soheila *et al* and Zhang *et al* (5-7).

The incidence of prostatitis has been increasing since 1995 (8), and chronic nonbacterial prostatitis (CNP) accounts for 90-95% of all prostatitis cases (9), with clinical symptoms including pelvic pain, frequent, urgent, painful micturition and increased nocturnal urination. In our previous study, it was reported that *Glycyrrhiza uralensis* exhibited therapeutic efficacy against CNP in rats (10). However, the effective parts of the aerial parts of *Glycyrrhiza uralensis* against CNP have not been identified, and the pharmacodynamic compounds and mechanisms remain unclear. Therefore, comparison of anti-CNP activity based on the extraction and enrichment of different parts of the aerial part of *Glycyrrhiza uralensis*, as well as determining the anti-CNP active components of the aerial part of *Glycyrrhiza uralensis* and their molecular mechanisms are vital.

Network pharmacology is based on the multi-layer disease-gene-drug network, and is used to predict drug targets and increase the efficiency of drug discovery (11). The concept of this research method is based on the view that traditional Chinese medicine (TCM) exerts improved overall therapeutic efficacy compared to the sum of its parts (12). Numerous studies have studied the interface between TCM and network pharmacology, and several methods have emerged to integrate the study of genes associated with disease and target information prediction, with the active components of TCM (13-16).

The present study applied network pharmacology (17) to obtain 23 flavonoids from the aerial part of *Glycyrrhiza uralensis*, identified CNP targets, and combined the biological target with the network to determine the modes of action and pathways of the anti-CNP constituents. This study provides insights into the pharmacokinetics of these ingredients with anti-CNP activity. The design of the network pharmacology study is illustrated in Fig. 1.

Materials and methods

Preparation of extracts from the aerial part of Glycyrrhiza uralensis. The original materials of the aerial part of *Glycyrrhiza uralensis* included the stems, leaves and fruit pods; the stem:leaf weight ratio was ~4:1. The materials were collected from Hedong Township, (Guazhou, Jiuquan, Gansu) in September 2016. The plants were 7 years old and cultivated for licorice production. Their aerial parts were identified by Professor Wang Wenquan of the Beijing University of Traditional Chinese Medicine (Beijing, China).

Laboratory animals and feeding conditions. Healthy male Sprague-Dawley (SD) rats (180-200 g; 8 weeks old; animal certificate no. SLXD-20200902021), were purchased from Beijing Weitong Lihua Experimental Animal Technology Co., Ltd.; the rats were fed a regular diet and had free access to drinking water. All rats were handled according to the National Guidelines for the Care and Use of Laboratory Animals, and all animal experiments were approved by the Animal Ethics Committee of the Chinese Academy of Medical Sciences and Institute of Medicinal Plant Development (approval no. SLXD-20200902021). For humane endpoints, the principle of minimal injury and trade-off was followed to minimize pain and meet the needs of the experiment. Euthanasia was performed when a wound did not heal after the construction of a prostatitis model in rats.

Experimental instruments and equipment. The following apparatus was used in the present study: Multiskan FC Enzyme Marker (Thermo Fisher Scientific, Inc.); UltiMate-3000 HPLC (Thermo Fisher Scientific, Inc.), Agilent SB-C18 column (250x4.6 mm, 5 μm) (Agilent Technologies, Inc.), N6000 ultraviolet spectrophotometer (Shanghai Yuke Instruments), FA 2004N analytical balance (Shanghai Yuke Instruments); RE-52 rotary evaporator (Shanghai Yarong Biochemistry Instrument Factory); 101-2 AB electrothermal blast dryer (Tianjin Tester Instrument Co., Ltd.); JJ-12J dehydrator (Wuhan Junjie Electronics Co., Ltd.); JB-P5 (Wuhan Junjie Electronics Co., Ltd.); RM2016 histopathological slicer (Shanghai Leica Instrument Co., Ltd.); JB-L5 freezing platform (Wuhan Junjie Electronics Co., Ltd.); KD-P stand (Zhejiang Jinhua Cody Equipment Co., Ltd.); DHG-9140A oven (Shanghai Huitai Instrument Manufacturing Co., Ltd.); 10212432C slides and coverslips (Jiangsu Shitai Experimental Equipment Co., Ltd.); NIKON ECLIPSE CI Orthopedic Optical Microscope (Nikon Corporation); NIKON DS-U3 imaging system (Nikon Corporation); MM823LA6-NS microwave oven (Midea Microwave Appliance Manufacturing Co., Ltd.); WD-9405A decolorization shaker (Beijing 61 Instrument Factory); TYXH-II vortex mixer (Tianyue Electronics); GT1001 composition pen (Gene Tech); and NIKON ECLIPSE TI-SR positive fluorescence microscope (Nikon Corporation). Other equipment included surgical scissors, tweezers, curved needles, surgical sutures and syringes.

Reagents and chemicals. The following reagents and test kits were used: Carrageenan (Beijing Solarbio Science and Technology Co., Ltd.; cat. no. 1202 A053); sodium cellulose (Tianjin Fuchen Chemical Reagent Factory); chloral hydrate (Tianjin Fuchen Chemical Reagent Factory); prostaglandin E2 (PGE2; cat. no. F2944-B), NF-κB (cat. no. F8592-A), nitric oxide (NO; cat. no. A012-1-1), induced NO synthase (iNOS; cat. no. A014-1-2), prostate-specific antigen (PSA; cat. no. F3343-B) and malondialdehyde (MDA; cat. no. A003-1-2) (Nanjing Institute of Bioengineering or Beijing Baioske Biomedical Technology Co., Ltd.); IL-1β (cat. no. GB11113), TGF-β (cat. no. GB11179), connective tissue growth factor (cat. no. 23936-1-AP), monocyte chemoattractant protein-1 (MCP-1; cat. no. GB11199), TNF-α (cat. no. GB13188-2), α-smooth muscle actin (α-SMA; cat. no. GB13044) all from Wuhan Seville Biotechnology Co., Ltd. or Thermo Fisher Scientific, Inc.; G1203EDTA (pH 9.0) antigen repair solution (Wuhan Google Biotechnology Co., Ltd.); G0002PBS buffer (Wuhan Google Biotechnology Co., Ltd.); EDTA (pH 8.0) antigen repair solution (Wuhan Google Biotechnology Co., Ltd.); G1202 citric acid (pH 6.0) antigen repair solution (Wuhan Google Biotechnology Co., Ltd.); AR1010 normal rabbit serum (Boster Biological Technology); G1004 hematoxylin dye solution (Wuhan Google Biotechnology Co., Ltd.); K5007 II (Dako; Agilent Technologies, Inc.); K5007 histochemical kit DAB chromogenic agent (Dako; Agilent Technologies, Inc.); acetonitrile (chromatographic purity), methanol (chromatographic purity) (Thermo Fisher Scientific, Inc.); formic acid (Beijing Chemical Plant); and Qianlukang (Zhejiang Kangenbei Pharmaceutical Co., Ltd.; cat. no. Z33020479; lot no. 190306).

Test substance preparation. For water extraction, 4.2 kg stem and leaf powder was decocted twice for 2 h at 100˚C and was then concentrated. A total of 1 g extract was equivalent to 6.33 g raw product. For ethanol extraction, 17.8 kg stem and leaf powder was extracted twice for 17 min in 70% ethanol at 70˚C and was then concentrated. A total of 1 g extract was equivalent to 7.8 g raw product.

HPLC analysis of the components in the test substance. The chromatographic conditions were as follows: Agilent SB-C18 column (250x4.6 mm, 5 μm), acetonitrile as the mobile phase A, and 0.5% formic acid-water as the mobile phase B. The elution gradient is indicated in Table I. The column temperature

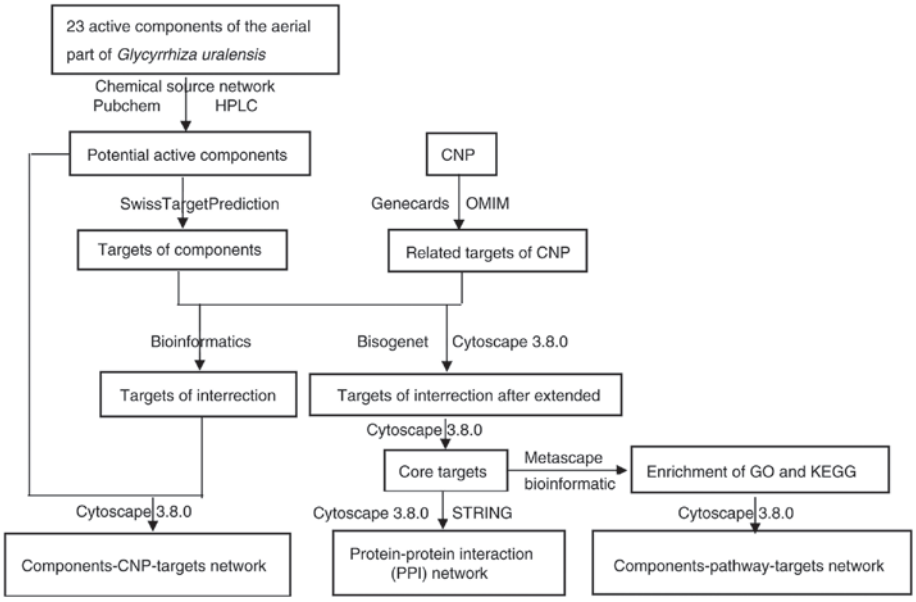

Figure 1. Research method of the anti-CNP mechanism of the aerial part of *Glycyrrhiza uralensis* based on network pharmacology. CNP, chronic nonbacterial prostatitis; GO, Gene Ontology; KEGG, Kyoto Encyclopedia of Genes and Genomes; HPLC, high-performance liquid chromatography; STRING, Search Tool for the Retrieval of Interacting Genes/Proteins.

was set at 30˚C with a flow rate of 0.8 ml/min. The detection wavelength was 280 nm, and the injection volume was 10 μl.

Sample solutions were prepared by accurately weighing 1 g sample powder in a conical flask, adding 10 ml 70% (v/v) ethanol, weighing the mixture, ultrasonicating (100 W) for 30 min, cooling it, reweighing, making up the lost volume by topping it up with 70% (v/v) ethanol, shaking by hand, filtering and collecting the filtrate.

Pharmacodynamics study. A total of 40 clean, healthy male SD rats (180-200 g; 8 weeks) were used in the present study. To produce the CNP model, the rats were anesthetized using 10% chloral hydrate (300 mg/kg) by intraperitoneal injection. The rats were considered completely anesthetized when the rats' paws were pressed hard and the rats did not exhibit a response. No symptoms of peritonitis were observed in the rats after anesthesia; thus, the skin on the middle of the lower abdomen was disinfected and an incision of ~2 cm was aseptically made. Then, 0.1 ml carrageenan in saline was injected into the rats in the treatment group, while an equal volume of saline was injected into the rats in the control group. The incisions were closed with sutures, and the wounds were disinfected with iodine. After producing the model, the rats were then treated accordingly. A total of 24 rats with induced prostatitis were randomly divided into three different treatment groups: Water extract (1,000 mg/kg), ethanol extract (1,000 mg/kg) and Qianzhikang (586 mg/kg) groups; each group consisted of 8 rats. Rats in the five treatment groups were administered the drugs once daily. The blank control consisted of 8 sham-operated rats. The control and model rats received 0.7% CMC-Na (20 ml/kg) by continuous gavage for 30 days via gastric administration. In our previous study, 1,000 mg/kg of licorice was determined to induce anti-CNP activity. The dose administered to each rodent was obtained by flavonoid conversion.

A total of 30 days later, the rats (~300 g) were anesthetized. Then, 10 ml blood was collected from each rat's abdominal aorta. After collecting the blood, each rat was euthanized by cervical vertebrae dislocation; rats were considered dead after the heartbeat ceased. The organs were collected immediately after confirmation of death.

Detection of body weight and organs of rats. By day 30, rat hair, diet, activity, body weight, visceral lesions and visceral index (combination of prostate index, thymus gland index, cardiac index, kidney index, adrenal index and spleen index) were observed and measured. The visceral index as a percentage was calculated as: [weight of the viscera (g)/weight of the body (g)] x 100.

Multigroup comparisons of the means were carried out using a one-way ANOVA with a post hoc Duncan's test.

Assessment of the prostate tissue in rats

Hematoxylin and eosin (HE) staining of prostate tissue. Patients with CNP show glandular atrophy, glandular epithelial cell shedding, necrosis, interstitial lymphocytic infiltration, tissue fibrosis hyperplasia and other lesions (18). HE staining can be used to observe tissue structure, inflammatory cell infiltration and to analyze the pathological morphology of prostate tissue.

The prostate tissue was fixed in 4% paraformaldehyde for 30 h at room temperature. After dressing the fixed prostate tissue with a scalpel, the tissue was dehydrated with anaerobic ethanol, paraffin embedded, sliced to 4-6 μm. The steps were as follows i) Sections were deparaffinized in xylene for 5-10 min. ii) Sections were moved into a mixture of xylene and pure alcohol (1:1) for about 5 min. iii) Sections were hydrated in 100, 95, 85 and 70% alcohol solutions for 2-5 min. iv) Tissues were stained with hematoxylin for 5-15 min. v) Excess dye was washed and sections were placed in 0.5-1% hydrochloride alcohol (70% alcohol prepared) for 10 sec. vi) Sections were rinsed with running water for 15-30 min. vii) Sections were stained with 0.1-0.5% eosin for 1-5 min. viii) Sections were dehydrated with 70, 85, 95 and 100% alcohol at all levels for

Table I. Flow phase gradient elution conditions.

Time, min	Acetonitrile, %	Formic acid-water, %
0-5	10→15	90→85
5-22	15→22	85→78
22-40	22→40	78→60
40-52	40→50	60→50
52-76	50→85	50→15
76-77	85→10	15→90
77-87	10→10	90→90

2-3 min. ix) Sections were cleared using xylene (secondary) for ~10 min. x) Sealing, excess xylene around the section was wiped without allowing the fixative to dry, and then the slide was placed quickly in an appropriate amount of neutral gum, to allow the cover glass to be sealed. All of the above steps were performed at room temperature. The nucleus was stained blue, and the cytoplasm was red.

Observation and evaluation methods of HE slices. After HE staining of the prostate tissues, the pathological changes of the tissue were observed under a light microscope (magnification, x400), and the morphology of prostate glands, infiltration of inflammatory cells in prostate stroma and hyperplasia of fibrous tissue were recorded. Based on previous findings (19), the pathological changes of tissues were graded and the scoring criteria were established as follows: i) Morphology of glands scoring: 2 points, the prostate gland was complete, glandular epithelial cells arranged neatly, folded into the lumen to form a fold; 4 points, glandular epithelium was damaged, and glandular epithelial folds were reduced; and 6 points, the glandular epithelium was severely damaged and deformed, and the glandular epithelium folds were reduced or absent. ii) Degree of infiltration of inflammatory cells: 2 points, occasional inflammatory cell infiltration in the glandular interstitium; 4 points, moderate inflammatory cell infiltration in the glandular stroma; and 6 points, extensive inflammatory cell infiltration in the glandular stroma. iii) Degree of fibrous tissue hyperplasia: 2 points, occasional fibrous tissue hyperplasia; 4 points, moderate fibrous tissue hyperplasia; and 6 points, extensive fibrous tissue hyperplasia.

Masson staining of prostate tissue. Prostate tissue in patients with CNP is often accompanied by a large number of fibrous connective hyperplasia and a hard texture (20). Masson staining can dye the fibrous tissue blue, which is used to analyze the degree of fibrosis and hyperplasia of prostate tissue.

After dissecting the rats, the prostate tissue was taken and immediately fixed as described above. After the fixed prostate tissue was obtained with a scalpel, it was dehydrated, embedded in paraffin and sliced (4 μm thick). The following procedures were then performed: Sections were washed with distilled water and nucleus was stained with Weigert's hematoxylin (BIOSS, Beijing; cat. no. S0082-2) for 5-10 min, then washed with distilled water. Tissues were next stained with Ponceau de xylidine-acid fuchsin mixture (Gurr) for 5-10 min. Then sections were immersed in 2% aqueous glacial acetic acid solution for 2 min. Sections were differentiated with an aqueous solution of 1% phosphate-molybdate acid for 3-5 min. Then they were directly stained with light green SF yellowish (BIOSS, Beijing; cat. no. D10419) for 5 min and immersed for 2 min in aqueous 0.2% glacial acetic acid. Excess dye was wiped using 95% alcohol, then dehydrated using anhydrous alcohol and cleared using xylene, followed by sealing using the neutral gum, as described above. All of the above steps were performed at room temperature. The collagen fibers, mucus and cartilage were stained blue, muscle fibers, cellulose and red blood cells were stained red, and the nucleus was stained blue-black.

Image Pro-Plus 6.0 (Media Cybernetics) analysis software was used for quantitative analysis. A total of 5 non-overlapping fields were randomly selected for each slice. The degree of fibrosis in the prostate tissue was analyzed by calculating the area of positive staining (area) and the cumulative optical density (IOD). The larger the area of fibrosis and the IOD were, the higher the degree of fibrosis and hyperplasia in the prostate tissue was.

IHC staining of prostate tissue. The expression of inflammatory and fibrotic factors in the prostate tissue of patients with CNP is increased (21,22). IHC staining was used to analyze the distribution and content of certain inflammatory factors qualitatively and quantitatively in the tissue sections using specific antibodies (Rabbit antibodies). After dehydration of paraffin sections, sections were boiled in EDTA Antigen Repair Buffer (pH 9.0), and subsequently, the dewaxed sections were placed in repair fluid for 2 min. The sections were allowed to cool passively to room temperature. Slides were removed and washed with PBS three times, 5 min per wash. Sections were soaked in 3% H_2O_2 for 20 min and washed with PBS three times, 5 min prewash. Tissues were next incubated with rabbit serum (cat. no. AR1010; Boster) or 10 min at room temperature. Next, tissues were incubated with the primary antibodies: MCP-1 antibody (cat. no. 45071; Signalway Antibody LLC; 1:100), TNF-α Monoclonal antibody (cat. no. 44073; Signalway Antibody LLC; 1:100), TGF-β antibody (cat. no. 5559-100; BioVision, Inc.; 1:200), α-SMA Monoclonal Antibody (cat. no. 40482; Signalway Antibody; 1:200)] all diluted in PBS (cat. no. G0002; Cellway) at 37˚C for 1-2 h, followed by incubation with the goat anti-rabbit IgG secondary antibodies (cat. nos. ZI215-1 or ZS402-2; ZOMANBIO; 1:1,000) at 37˚C for 10-30 min, and the corresponding inflammatory factors in the tissue were dyed brownish/yellow to analyze the expression intensity (IOD value) of inflammatory factors in prostate tissue.

Selection of observation indicators. Rat hair, diet, activity, body weight, visceral lesions and the viscera index were measured and observed during the pharmacological experiments. The viscera index comprised the prostate and thymus indices. Additionally, the expression levels of the serum detection factors MCP-1, TNF-α, PGE2 and NF-κB were determined.

To observe and evaluate the hair, diet, activity, body weight, organ lesion and organ index of rats during the pharmacological experiments, and to evaluate the prostate gland morphology, inflammatory factor infiltration, fibrosis hyperplasia, expression of inflammatory factor and fibrotic factor using HE staining, Masson staining and IHC staining, the expression of MCP-1, TNF-α, PGE2 and NF-κB in rat serum was measured.

Table II. The 23 chemical components in the aerial parts of *Glycyrrhiza uralensis*.

No.	CAS	Name	Chemical formula	Type
MOL 1	491-70-3	Luteolin	$C_{15}H_{10}O_6$	Flavone
MOL 2	480-41-1	Naringenin	$C_{15}H_{12}O5$	Flavone
MOL 3	446-72-0	Genistein	$C_{15}H_{10}O5$	Isoflavone
MOL 4	520-34-3	Diosmetin	$C_{16}H_{12}O_6$	Flavone
MOL 5	480-19-3	Isorhamnetin	$C_{16}H_{12}O_7$	Flavone
MOL 6	480-39-7	Pinocembrin	$C_{15}H_{12}O_4$	Flavonone
MOL 7	548-83-4	Galangin	$C_{15}H_{10}O_5$	Flavonol
MOL 8	116709-70-7	Glycyrrhisoflavone	$C_{20}H_{18}O_6$	Prenylated Isoflavone
MOL 9	51225-30-0	Wighteone	$C_{20}H_{18}O_5$	Prenylated Flavonoid
MOL 10	109605-79-0	Topazolin	$C_{21}H_{20}O_6$	Prenylated Flavonoid
MOL 11	486-66-8	Daidzein	$C_{15}H_{10}O_4$	Isoflavone
MOL 12	34221-41-5	Retrochalcone	$C_{16}H_{14}O_4$	Chalcone
MOL 13	485-72-3	Formononetin	$C_{16}H_{12}O_4$	Isoflavone
MOL 14	51938-32-0	Schaftoside	$C_{26}H_{28}O_{14}$	Flavonoid Dioxide
MOL 15	3681-99-0	Puerarin	$C_{21}H_{20}O_9$	Isoflavone Oxyglycoside
MOL 16	23666-13-9	Vicenin-2	$C_{27}H_{30}O_{15}$	Flavonoid Double Carbon Glycoside
MOL 17	52012-29-0	Isoschaftoside	$C_{26}H_{28}O_{14}$	Flavonoid Dioxide
MOL 18	21637-25-2	Isoquercitrin	$C_{21}H_{20}O_{12}$	Flavonol Glycoside
MOL 19	5041-81-6	Isoliquiritin	$C_{21}H_{22}O_9$	Chalcone Oxide
MOL 20	63631-41-4	Arvensan	$C_{17}H_{18}O_4$	Benzopyrone
MOL 21	520-18-3	Kaempferol	$C_{15}H_{10}O_6$	Flavone
MOL 22	139163-15-8	Uralenol	$C_{20}H_{18}O_7$	Prenylflavonol
MOL 23	126716-36-7	Gancaonin I	$C_{21}H_{22}O_5$	Prenylated Flavonoid

By analyzing the effect of each administration group on the expression of serum inflammatory factors, the anti-CNP activity of different extraction and separation components on the aerial part of *Glycyrrhiza uralensis* was evaluated, and the basis of pharmacodynamics was determined.

Methods of staining IHC sections. The prostate tissue was fixed in 4% paraformaldehyde for >24 h at room temperature. After the fixed prostate tissue was repaired with a scalpel, the prostate tissue was dehydrated with distilled water for 1 h, embedded in paraffin and sliced into 4 μm thick sections. After dewaxing, antigen retrieval was performed using EDTA antigen repair buffer (pH 9.0) and sections were placed in a boiling water bath. After boiling for 15 min, tissues were allowed to cool passively to room temperature. The endogenous peroxidases were quenched using 3% hydrogen peroxide solution. The primary and secondary antibodies as well as DAB chromogenic solution were added, and the nucleus was re-stained with Harris hematoxylin for 3-15 min at room temperature. The slices were dehydrated with distilled water for 1 h, cleared until they were transparent, dried and sealed using neutral gum. The positive expression in tissue appeared brownish/yellow.

Evaluation method of IHC sections. IHC staining can dye the positively expressing tissue brownish/yellow. Image Pro-Plus software was used for quantitative analysis. A total of 5 non-overlapping fields of vision were randomly selected for each slice. The expression of related factors was analyzed by calculating the IOD of the positive staining area. The greater the IOD value, the greater the expression of the associated factors, which helps to determine the therapeutic effect of each drug on CNP.

Serum sampling and detection of serum inflammatory factor expression in rats. A total of 24 h after the final treatment, blood samples were obtained from the abdominal aorta, placed at 25±1˚C for 0.5 h, and centrifuged using a frozen centrifuge at 1,006 x g for 10 min; the supernatant was obtained (serum). Detection of inflammatory factors was performed according to the kit's instructions. The absorbance A was detected at 450 nm, and the content of each factor was, then, calculated.

Network pharmacology analysis

Target prediction of the 23 components in the aerial part of Glycyrrhiza uralensis. All structural formulae, based on the components of the aerial part of *Glycyrrhiza uralensis* determined previously (7), were introduced into SwissADME (swissadme.ch/) to screen for 17 chemical components (excluding Schaftoside, Puerarin, Vicenin-2, Isoschaftoside, Isoquercitrin, Isoliquiritin; Table II) that would exhibit gastrointestinal absorption and drug-like efficacy; at least two 'yes' in the drug-like efficacy predictions and gIabsortion absorption was considered 'High'. The levels of the 6 components (Schaftoside, Puerarin, Vicenin-2, Isoschaftoside, Isoquercitrin and Isoliquiritin) were higher than those for the 17 chemical components selected in SwissADME. Hence, the structures of the 23 components were imported into SwissTargetPrediction (swisstargetprediction.ch/). *Homo sapiens* was used as the research object and all other parameters were left as the system

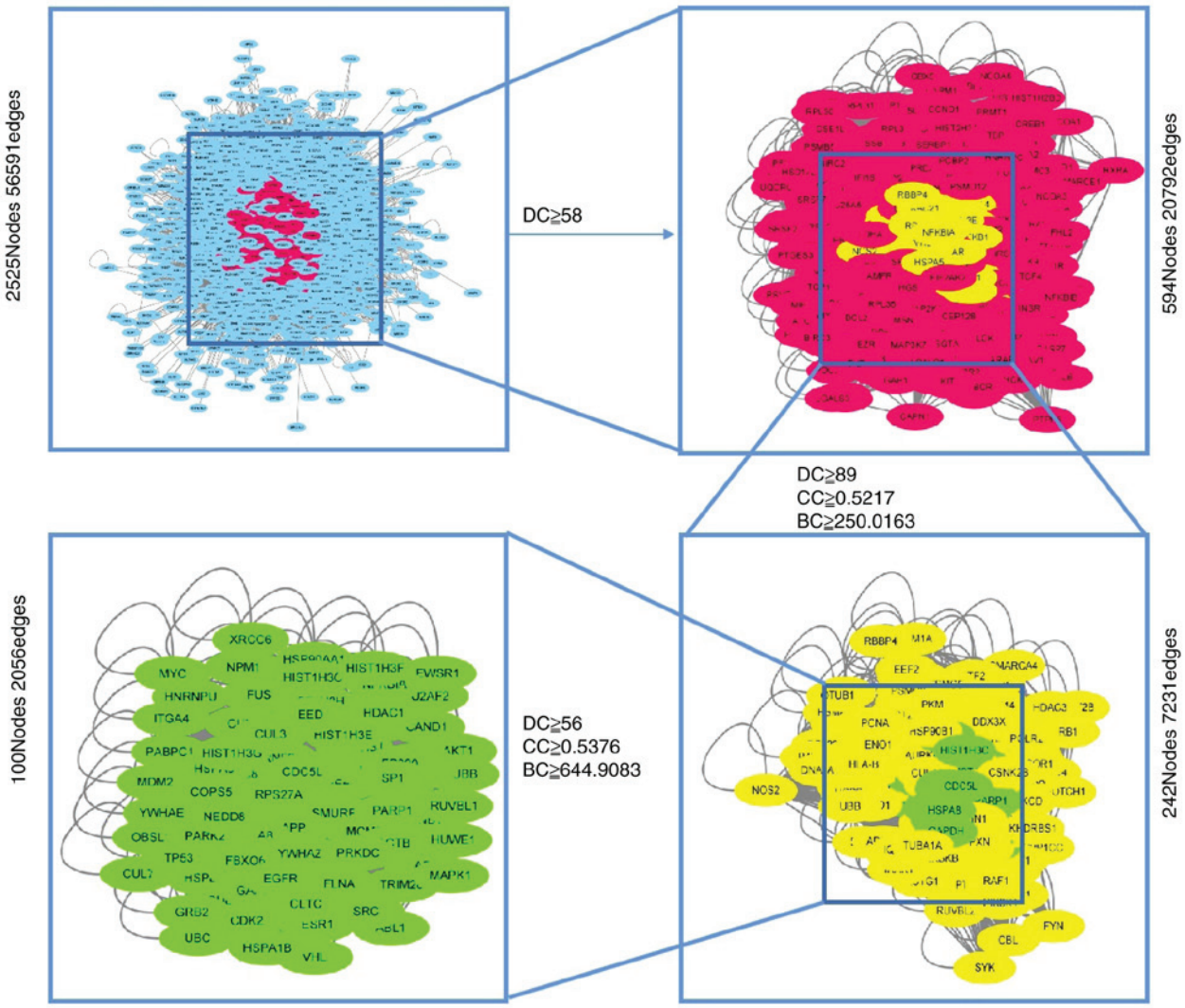

Figure 2. Core target screening flowchart. DC, degree centrality; BC, betweenness centrality; CC, closeness centrality.

defaults. The chemical components corresponding to human target proteins and their corresponding genes were noted and their targets were predicted.

CNP target prediction. CNP-related targets with 'Chronic Nonbacterial Prostatitis' were searched for in Genecards (genecards.org/) and in Gene Map in OMIM (omim.org/). The data obtained in Genecards and Gene Map were merged using Excel2016 (Microsoft Corporation). Data for the coinciding gene entries including the corresponding protein names and gene entry IDs were eliminated from the Excel spreadsheet to obtain data for genes and target proteins associated with CNP.

Construction of the component-CNP-target gene network. A Venn diagram was plotted in Bioinformatics (bioinformatics.psb.Ugent.be/webtools/Venn/) to obtain potential CNP-associated target genes for the 23 active compounds. The network was generated using Cytoscape version 3.8.0 (23) to illustrate the complex relationships amongst the genes, aerial part components and CNP. In the network, compounds, genes and CNP were represented by nodes, whereas their interactions were indicated by edges. The value for each node was calculated and represented as the number of edges linked to it. In this manner, the major nodes in the network were characterized. The probability that a component was a key ingredient in CNP treatment increased with node value.

Construction of the protein-protein interaction (PPI) networks. The targets of the chemical components and CNP were uploaded into the Cytoscape plug-in *Bisogenet* (24) to expand the target. The intersecting targets of the expanded chemical components and CNP were selected. Filtration of the 'Degree' median was performed twice to obtain network 1 whereas network 2 was obtained via a single filtration of the 'Degree', 'Closeness' and 'Betweenness' medians in network 1. Network 3 was obtained using a single filtration of the 'Degree', 'Closeness' and 'Betweenness' medians in network 2, and included 100 nodes and 2,056 edges. The screening flow chart is shown in Fig. 2. The 100 nodes were regarded as core targets and placed in Search Tool for the Retrieval of Interacting Genes/Proteins (STRING; tring-db.org/cgi/input.pl) to build the PPI interaction network. Cytoscape was used to construct and visualize the PPI network. 'Degree' refers to the number of nodal connections in the entire network and reflects the interactions amongst nodes. The 'Degree' value was proportional to the core target importance.

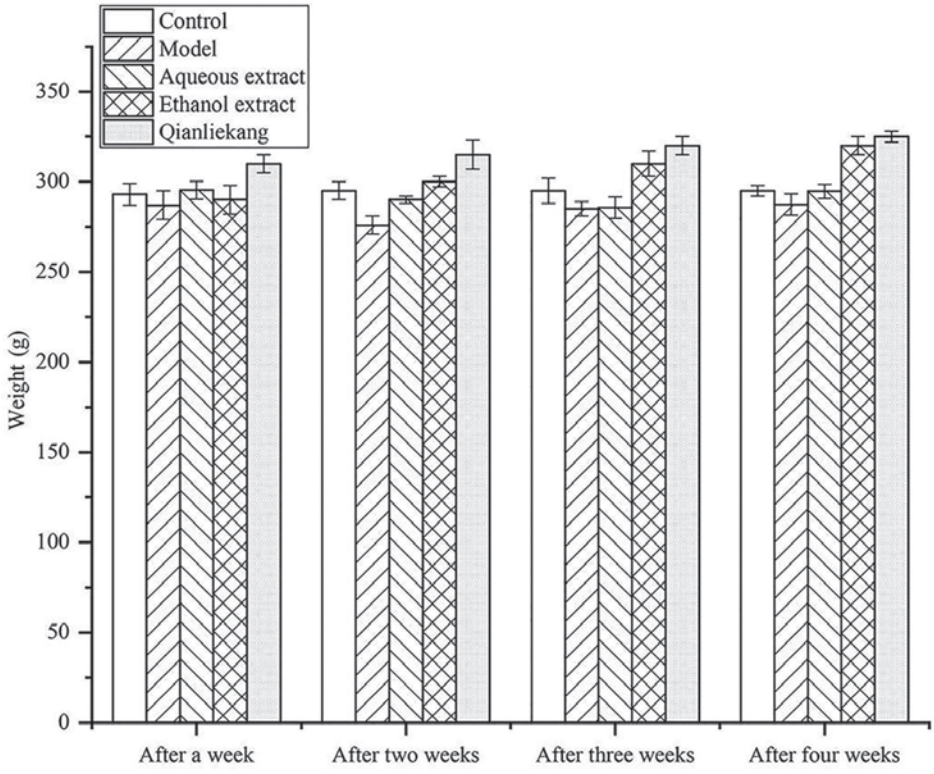

Figure 3. Effects of different extraction and enrichment parts on rat body weight (n=8).

Gene ontology (GO) and kyoto encyclopedia of genes and genomes (KEGG) pathway enrichment analyses. Metascape (metascape.org/gp/index.html#/main/step1) was used to process the data and visualize the results of the GO (25,26) enrichment and KEGG (27) pathway analyses. GO enrichment included biological processes (BP), molecular functions (MF) and cellular components (CC). KEGG enrichment identified the potential biological pathways and functions associated with the target. The minimum overlap was set to 3 and the P-value cutoff was set to 0. A minimum value of 1.5 indicated significant enrichment. The first 20 entries were selected, and the results were visualized using a Venn diagram (bioinformatics.psb.ugent.be/webtools/Venn/).

Construction of the chemical component-pathway-target network. The top 20 pathways were selected according to the number of genes on the KEGG pathways, corresponding to the 23 chemical components of the licorice aboveground part to the core targets, to build a chemical component-pathway-target network.

Statistical analysis. Data analysis was performed using SAS version 9.0 (University of *North Carolina*), Origin 2018 64 Bit (American OriginLab Corporation) and Excel 2016. A Kolmogorov-Smirnov test was used to determine the normality of distribution, and variance analysis was assessed using a one-way ANOVA with a post hoc Tukey's test. The HE staining score was analyzed using a non-parametric Kruskal-Wallis test with a Dunn's post hoc test, and the data are presented as box plots of the median and interquartile range. Multiple comparisons of the means in pharmacological experiments were performed using a one-way ANOVA with a post hoc Tukey's test. Each group of results consisted of 8 repeats. $P<0.05$ was considered to indicate a statistically significant difference.

Therefore, it is advised to reanalyze these data using non-parametric tests such as Kruskal-Wallis test with a Dunn's post hoc test, which do not assume that the analyzed data are continuous, and to also present the data as box plots of the median and interquartile range.

Results

Analysis of pharmacological experiments

Weight changes in rats. Changes in rat body weights are illustrated in Fig. 3. The average body weight of rats in each group was similar after 1 week of treatment with no significant differences compared with the control group. After 2 weeks of treatment, the body weight in the model group was slightly lower than that in the sham group, but not significantly different. After 4 weeks of treatment, the body weight in the ethanol extraction group was slightly lower than that in the other groups, but not significantly different.

These results showed that there was no significant difference in body weight amongst the groups during treatment, indicating that the drug did not affect the weight of the rats.

Effects of the different extraction and enrichment parts on viscera anatomy. The rats in the sham group were irritable, excited, hirsute and exhibited weight loss, with a red, glossy prostate tissue surfaces and soft, elastic glandular tissue. The prostate glands in the model group were red and swollen. There were no abnormal lesions in any other organ.

Effects of the different extraction and enrichment parts on the viscera index. Fig. 4 shows that the model group had a slightly higher prostate index than that of the sham group, but the

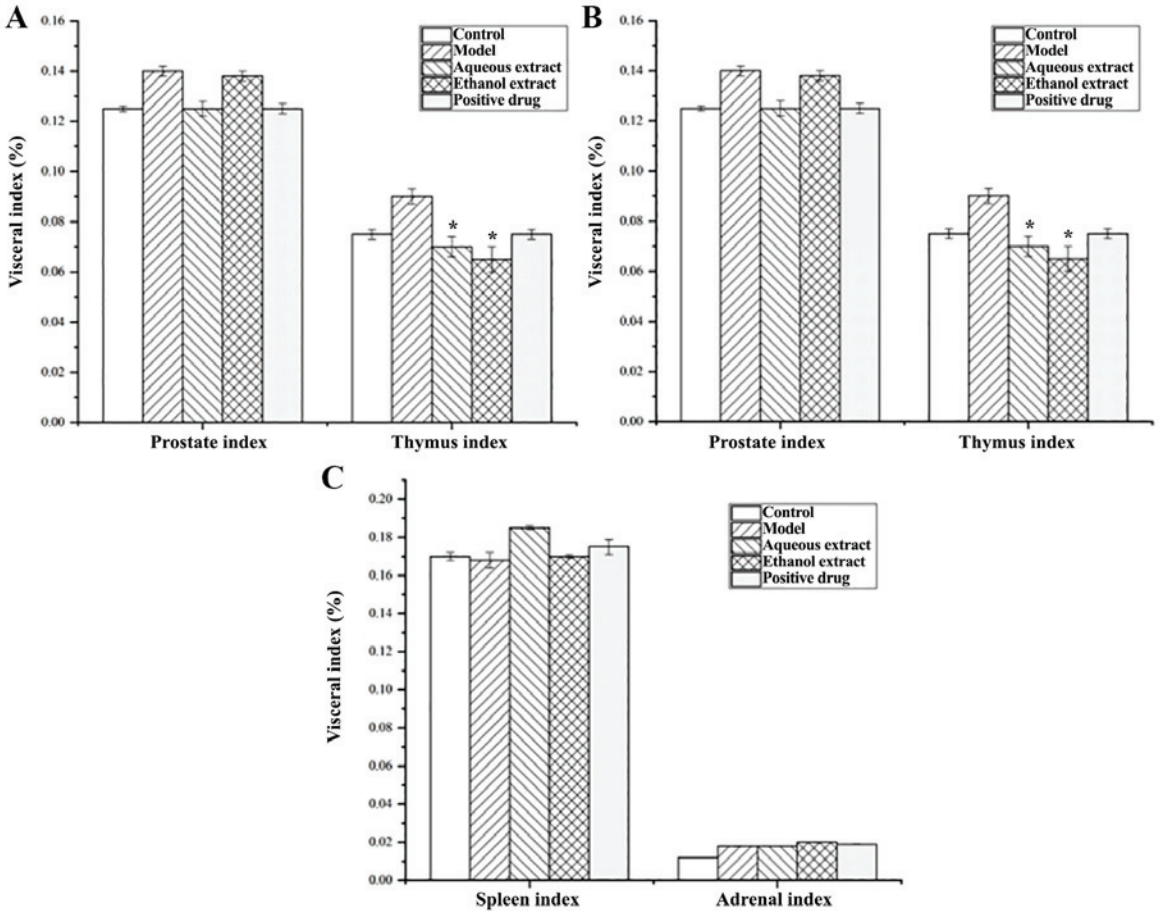

Figure 4. Effects of the different extractions and enrichment parts on the viscera index. (n=8). Effect of the different parts of *Glycyrrhiza uralensis* on the (A) prostate and thymus index; (B) the renal and cardiac index; and (C) the spleen and adrenal index. *P<0.05 vs. with the model group.

difference was not significant. The prostate index decreased in the water extraction groups, and the decrease was greater than that of the Qianluikang group, but not significantly different compared with the model group. Furthermore, the model group had a slightly higher thymus index than the sham operation group, but it was not significant. The thymus index of the water and ethanol extraction groups were significantly lower than that of the model group (all P<0.05).

In terms of renal index, there was no significant differences amongst the water extraction and Qianliekang groups compared with the model group, which was abnormally high; there was no significant difference between the cardiac, spleen and adrenal indices.

These results show that the organs most likely to be affected by CNP were the prostate and thymus; the water extraction groups showed a decreasing trend of prostate index and thymus index compared with the model group.

Pathological morphology of prostate tissue. The HE-stained pathological sections of the rat prostate tissues are shown in Fig. 5A. The prostate gland of rats in the sham group was intact without atrophy, and the single-layer cell structure of the glandular epithelium was also intact. There was no inflammatory cell infiltration, no fibrous tissue hyperplasia and abundant secretion in the glandular space. In the model group, the prostate gland of rats was severely deformed, the gland was atrophied and the gland epithelium was exfoliated and necrotic. There was extensive inflammatory cell infiltration in the gland stroma, and the secretions in the gland cavity were reduced, whilst some were colorless. The prostate glands of rats in the water and alcohol extraction groups were slightly deformed, significant inflammatory cell infiltration was observed and the secretions in the glands were slightly reduced. In summary, the inflammatory cells in the glandular space of the water, alcohol and Qianliekang groups were reduced to varying degrees, and the most obvious reductions were observed in the water groups.

The HE staining scores of the prostate tissue in the rats are shown in Fig. 5B-D. The results showed that compared with the sham group, the scores of gland morphological deformation, inflammatory cell infiltration and fibrous tissue hyperplasia in the model group were increased. In terms of prostate gland morphology in rats, compared with the model group, the scores of each administration group were decreased, and the decrease in the alcohol extraction group was the most significant. In terms of inflammatory cell infiltration in the prostate tissue of rats, compared with the model group, the scores of each administration group were reduced to varying degrees; amongst these, the decrease in the water extraction group was the most notable, and was lower than that in the Qianliekang group. In terms of fibrosis and hyperplasia of prostate tissue in rats, compared with the model group, each administration group exhibited differing degrees of reduction; amongst them, the decrease in the water extraction group was the most notable, and was lower than that in the Qianliekang group.

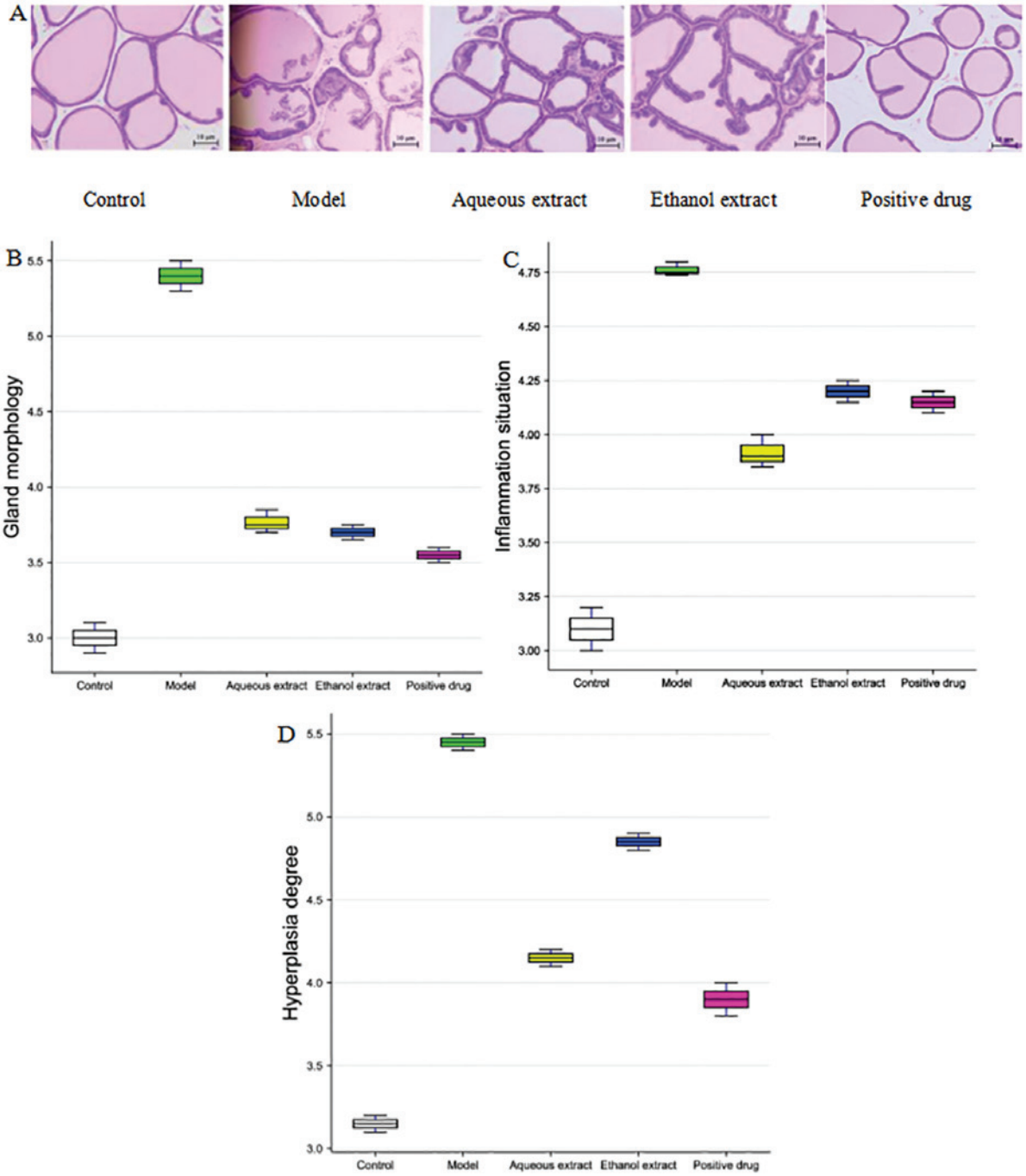

Figure 5. Hematoxylin and eosin staining following treatment with the different extraction and enrichment parts. (A) Hematoxylin and eosin staining results following treatment with the different extraction and enrichment parts. Magnification, x400. (B) Gland morphology following treatment with the different extraction and enrichment parts (n=8). Degree of (C) inflammation and (D) hyperplasia following treatment with the different extraction and enrichment parts (n=8).

Thus, the aqueous extract, ethanol extract and Qianliekang groups all tended to improve the morphology of prostate gland in rats. The water extraction exhibited the most potent mitigation on the hyperplasia of prostate tissue in rats.

Analysis of the degree of fibrosis in prostate tissue. Masson stained sections of rat prostate tissue are shown in Fig. 6A. There was no obvious hyperplasia in the sham group. The blue area of the prostate tissue in the model group was visible and large, and fibrosis was observed. Compared with the model group, the blue area in each administration group was significantly reduced, and that in the water extraction group is the most significantly decreased.

The calculation of Masson staining IOD and area of fibrosis hyperplasia in rat prostate tissues are shown in Fig. 6B and C; the larger the value, the greater the degree of fibrosis hyperplasia. Hyperplasia of prostate tissue in the model group was serious, and significantly higher than that in the sham operation group ($P<0.05$). i) In terms of the IOD of prostate tissues in rats, compared with the model group, each treatment reduced it by varying degrees, amongst them, the water extraction groups resulted in significant decreases ($P<0.05$). ii) Compared with the model group, the area of fibrosis hyperplasia in the prostate tissues of rats in each administration group was decreased to varying degrees ($P<0.05$).

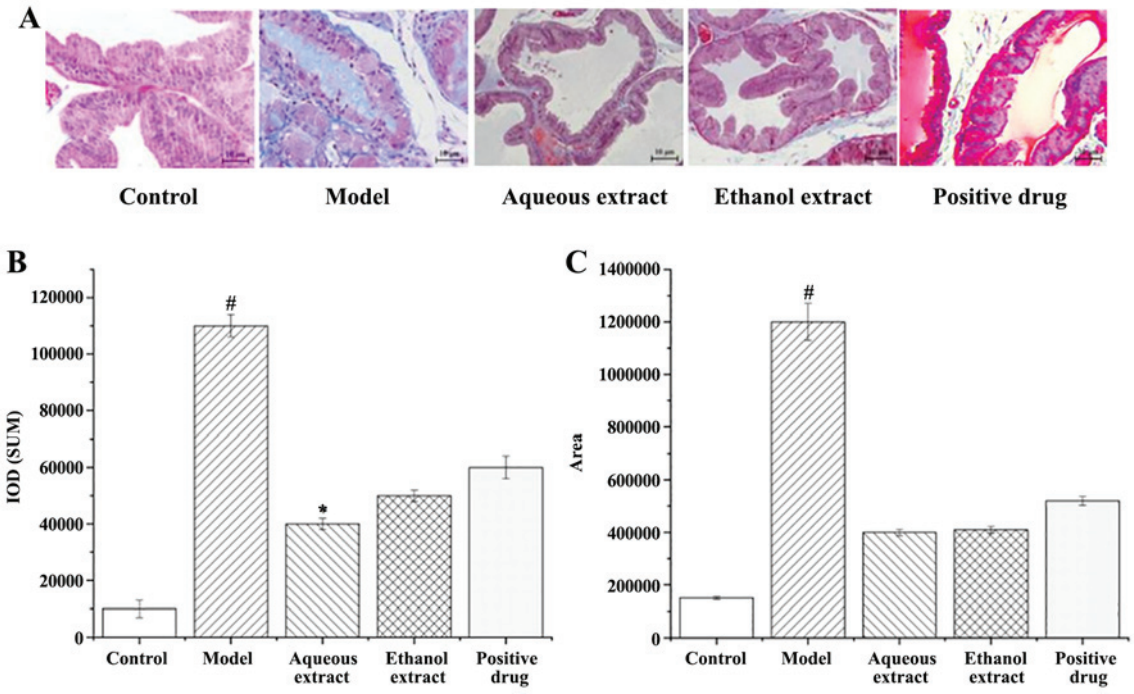

Figure 6. Masson staining analysis following treatment with the different extraction and enrichment parts. (A) Masson staining results following treatment with the different extraction and enrichment parts. Magnification, x400. (B) Cumulative IOD following treatment with the different extraction and enrichment parts (n=8). (C) Fibrotic areas following treatment with the different extraction and enrichment parts (n=8). #P<0.05 vs. sham group; *P<0.05 vs. model group. IOD, integrated optical density.

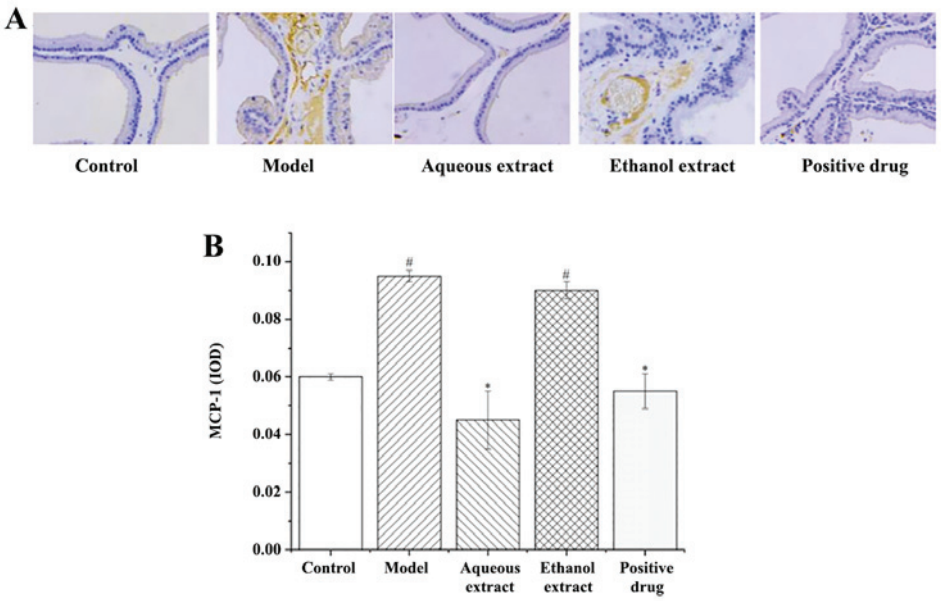

Figure 7. MCP-1 immunohistochemical staining following treatment with the different extraction and enrichment parts. (A) MCP-1 immunohistochemical staining. Magnification, x400. (B) Effects of the different extraction and enrichment parts on MCP-1 expression in rat prostates (n=8). #P<0.05 vs. sham group; *P<0.05 vs. model group. MCP-1, monocyte chemoattractant protein-1; IOD, integrated optical density.

In summary, the degree of prostatic fibrosis and hyperplasia in the administration group decreased to varying degrees, and the water extraction group showed the best results.

Analysis of expression intensity of inflammatory factors in prostate tissues

MCP-1 expression in prostate tissues. The results of MCP-1 expression in rat prostate tissues (IHC staining sections) are shown in Fig. 7A. The expression of MCP-1 in each group was as follows: i) Sham group, there was no brown granules in the cytoplasm and no MCP-1 positive expression; ii) model group, a large area of brown granules was distributed in the cytoplasm, MCP-1 positive expression was notably present; iii) ethanol extraction, the presence of the brownish yellow granules in the cytoplasm was significantly reduced compared with the model group, with some positive expression of MCP-1;

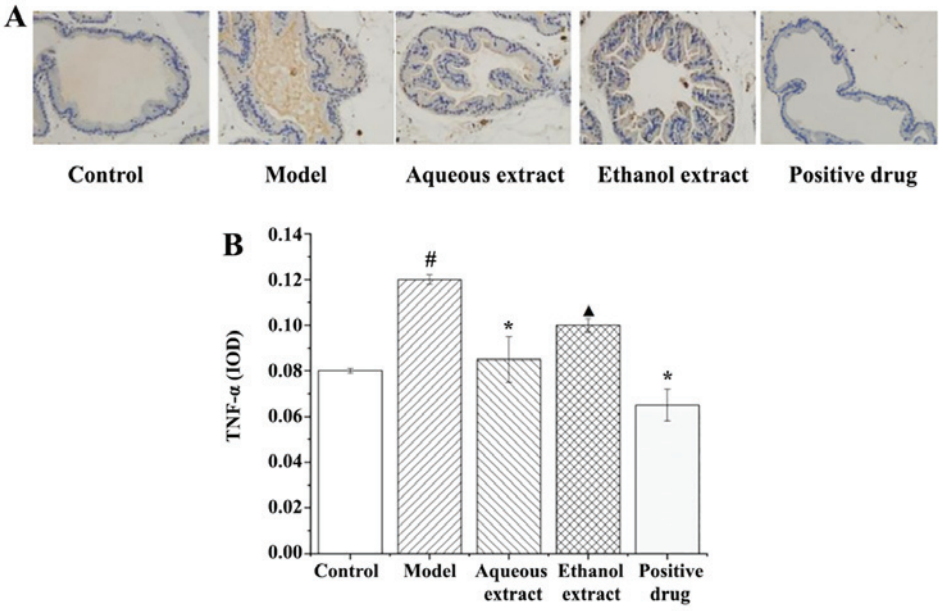

Figure 8. TNF-α immunohistochemical staining following treatment with the different extraction and enrichment parts. (A) TNF-α immunohistochemical staining. Magnification, x400. (B) Effects of different extraction and enrichment parts on TNF-α expression in rat prostates (n=8). #P<0.05 vs. sham group; *P<0.05 vs. model group; ▲P<0.05 vs. Qianliekang group. IOD, integrated optical density.

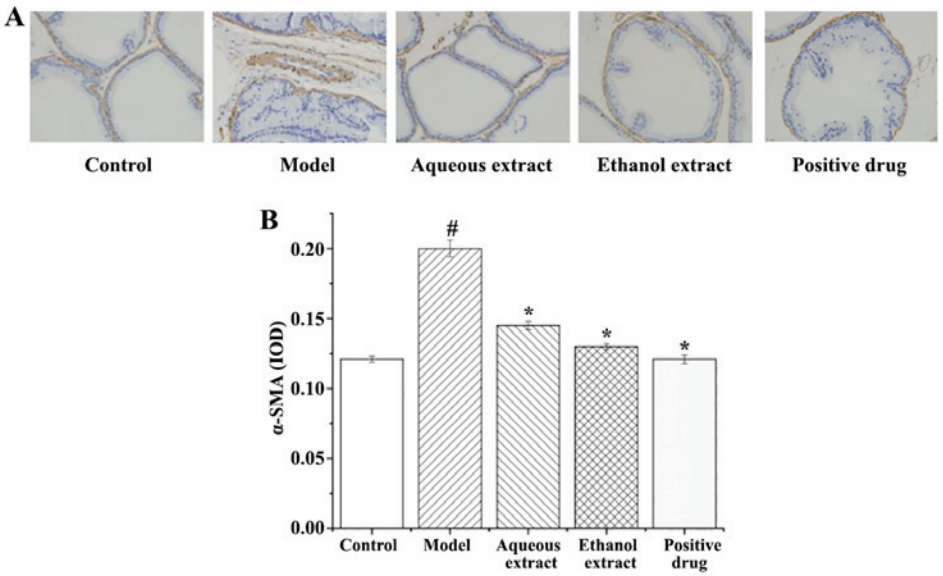

Figure 9. Results of α-SMA immunohistochemical staining in different extraction and enrichment parts. (A) Results of α-SMA immunohistochemical. Magnification, x400. (B) Effects of different extraction and enrichment parts on α-SMA expression in rat prostates (n=8). #P<0.05 vs. sham group; *P<0.05 vs. model group. α-SMA, α-smooth muscle actin. IOD, integrated optical density.

iv) water extraction and Qianliekang groups, there were only a few brownish yellow granules present in the cytoplasm, and the positive expression of MCP-1 was significantly lower than that in the model group.

The results of analysis of MCP-1 expression in rat prostate tissues are shown in Fig. 7B. The results showed that: i) The average optical density of MCP-1 in the model group was significantly higher than that in the sham group (P<0.05); ii) compared with the model group, the expression of MCP-1 in each administration group showed a decreasing trend, and the water extraction and Qianliekang groups were significantly lower (P<0.05); iii) the expression levels of MCP-1 in the water extraction group were lower than those in the Qianliekang group, and the expression levels of MCP-1 in the water extraction group were the lowest.

In summary, the water extract and Qianliekang groups could significantly reduce the expression of MCP-1 in rat prostate tissues, and the water extract group showed the best results.

TNF-α expression in prostate tissues. The results of TNF-α expression in rat prostate tissues (IHC staining sections) are shown in Fig. 8A, and they clearly illustrate that the expression of TNF-α in each group exhibited the following characteristics:

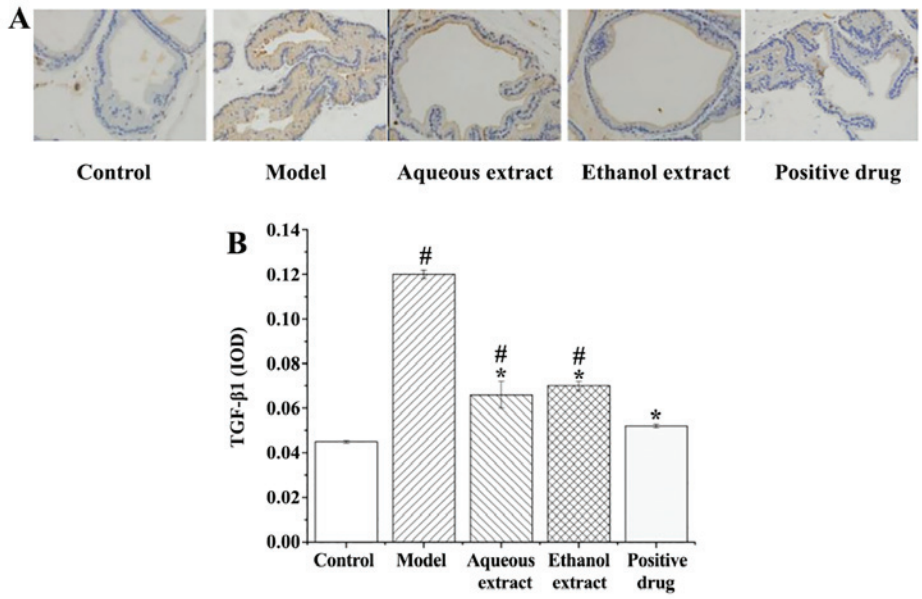

Figure 10. Results of TGF-β1 immunohistochemical staining following treatment with the different extraction and enrichment parts. (A) Results of TGF-β1 immunohistochemical staining. Magnification, x400. (B) Effects of different extraction and enrichment parts on TGF-β1 expression in rat prostate (n=8). #P<0.05 vs. sham group; *P<0.05 vs. model group. IOD, integrated optical density.

i) in the sham group, there was no brownish yellow granules in the cytoplasm, and no positive expression of TNF-α; ii) model group, a large area of brownish yellow granules was distributed in the cytoplasm, and the positive expression of TNF-α was notably present; iii) ethanol extract group, there were some brown granules in the cytoplasm, and TNF-α positive expression was strong; iv) water extraction and Qianliekang groups, there were only a few brownish yellow granules in the cytoplasm, and the positive expression of TNF-α was significantly lower than that in the model group.

The analysis results of TNF-α expression in rat prostate tissues are shown in Fig. 8B. The results showed that: i) The average optical density of TNF-α in the model group was significantly higher than that in the sham group (P<0.05); ii) compared with the model group, the expression levels of TNF-α in each administration group showed a decreasing trend, and the expression levels of TNF-α in the water extraction and Qianliekang groups was significantly decreased (P<0.05); iii) the expression levels of TNF-α in the ethanol extraction group were significantly higher than those in the Qianliekang group (P<0.05).

In summary, water extract and Qianliekang could significantly reduce the expression of TNF-α in rat prostate tissues, and Qianliekang showed the best results.

α-SMA expression in prostate tissues. α-SMA expression in rat prostate tissues (IHC staining sections) are shown in Fig. 9A. The expression of α-SMA in each group exhibited the following characteristics: i) Sham group, there were only a few brownish yellow granules in the smooth muscle, with less positive expression of α-SMA; ii) in the model group, smooth muscle exhibited large areas of brown particles, α-SMA positive expression was notably present; iii) the brownish yellow granules in the smooth muscle of each group were reduced to varying degrees, and the positive expression of α-SMA was significantly lower than that in the model group.

The analysis of α-SMA expression in the rat prostate tissues are shown in Fig. 9B. The results showed that: i) Expression of α-SMA in the model group was significantly higher than that in the sham group (P<0.05); ii) compared with the model group, the expression of α-SMA in each group was significantly decreased.

TGF-β1 expression in prostate tissues. TGF-β1 expression in rat prostate tissues (IHC staining sections) are shown in Fig. 10A. TGF-β1 expression in each group exhibited the following characteristics: i) Sham group, there were only a few brownish granules in the glands, and less positive expression of TGF-β1; ii) model group, large area of brownish yellow granules distributed in the glands, and positive expression of TGF-β1 was notably present; iii) water and ethanol extraction groups, the number of brownish yellow granules in the cytoplasm was decreased compared with the model group, with some positive expression of TGF-β1; iv) Qianliekang group, only a few brownish granules in the cytoplasm, TGF-β1 positive expression was significantly lower than the model group.

The analysis of TGF-β1 expression in the prostate tissues of rats is shown in Fig. 10B. The results showed that: i) TGF-β1 expression in the model group was significantly higher than that in the sham group (P<0.05); ii) compared with the model group, the expression levels of TGF-β1 in each group were significantly lower.

Thus, each concoction/drug significantly reduced the expression of TGF-β1 in rat prostate tissues, and the water group exhibited the most prominent effect.

Effects of different extraction parts on serum inflammatory factor expression in rats

Expression of MCP-1. The expression of MCP-1 in the serum of rats in each group is shown in Fig. 11A: i) Expression of MCP-1 in the serum of rats in the model group was significantly higher than that in the sham group (P<0.05); ii) compared

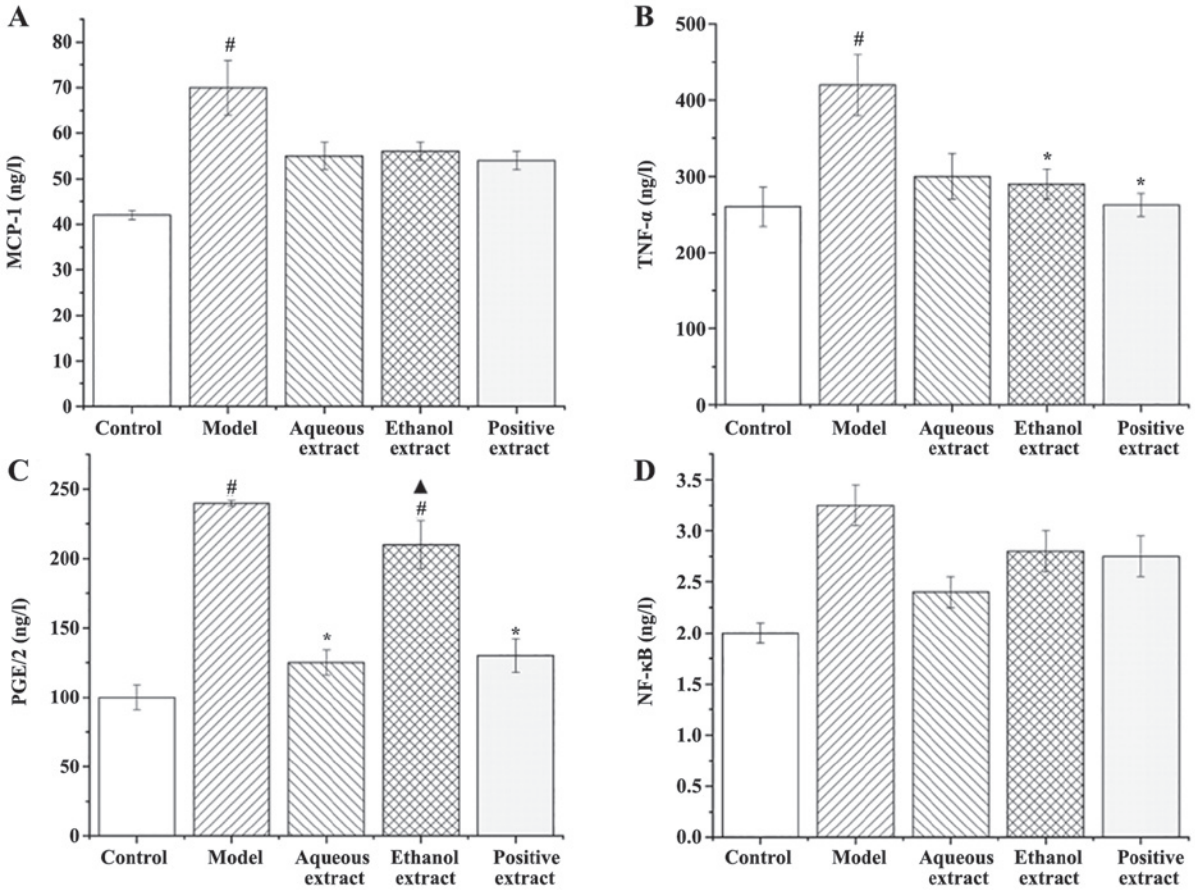

Figure 11. Effects of the different extraction and enrichment parts on serum inflammatory factor expression in rats. Effects of different extraction and enrichment parts on serum (A) MCP-1, (B) TNF-α, (C) PGE2 and (D) NF-κB expression in rats (n=8). #P<0.05 vs. sham group; *P<0.05 vs. model group; ▲P<0.05 vs. Qianliekang group. MCP-1, monocyte chemoattractant protein-1; PGE2, prostaglandin E2.

with the model group, the expression levels of MCP-1 in each administration group showed a decreasing trend.

Expression of TNF-α in serum. The expression of TNF-α in the serum of rats in each group is shown in Fig. 11B: i) Expression of TNF-α in the serum of rats in the model group was significantly higher than that in sham group (P<0.05); ii) compared with the model group, the expression of TNF-α in each administration group was decreased to varying degrees, and the decrease observed in the ethanol extraction and Qianliekang groups was significant (P<0.05).

In summary, the ethanol extract and Qianliekang groups significantly reduced the expression of serum TNF-α in CNP rats.

Expression of serum PGE2. The expression levels of PGE2 in the serum of rats in each group is shown in Fig. 11C: i) The expression levels of PGE2 in the serum of rats in the model group were significantly higher than that in the sham operation group (P<0.05); ii) compared with the model group, the PGE2 expression levels in the water extraction and Qianliekang groups were significantly decreased (P<0.05), and the PGE2 expression levels in the ethanol extraction group was also decreased, but not significantly compared with the model group; iii) the expression of PGE2 in the ethanol extract group was significantly higher than that in the Qianliekang group (P<0.05). There was no significant difference in the expression of PGE2 between the water extraction group and Qianliekang group, although it was lowest in the Qianliekang group. In summary, water extract could significantly reduce the serum PGE2 expression of CNP rats.

Expression of NF-κB in serum. The expression of NF-κB in the serum of rats in each group is shown in Fig. 11D: i) The expression of NF-κB in the serum of rats in the model group was slightly higher than that in the sham group, but the difference was not significant; ii) compared with the model group, the expression levels of NF-κB in each administration group decreased to varying degrees, but the decrease was not significant.

Network pharmacology analysis

Prediction of the targets of the 23 components of the aerial part of Glycyrrhiza uralensis. A total of 17 chemical components with strong gastrointestinal absorption and drug-like properties were identified, all of which were either flavonoids or flavonoid glycosides. Compositional analysis of the components in the test substance showed that this plant material contained high levels of six flavonoid glycosides These six components were part of the 23 components previously determined to be present in the aerial part of *Glycyrrhiza uralensis*; their gastrointestinal absorption and drug-like properties were poor, but their levels were high in the subjects (Fig. 7). The structural formulae of the 23 components were introduced into SwissTargetPrediction to obtain relevant targets. The 23 chemical components had 501 predicted targets.

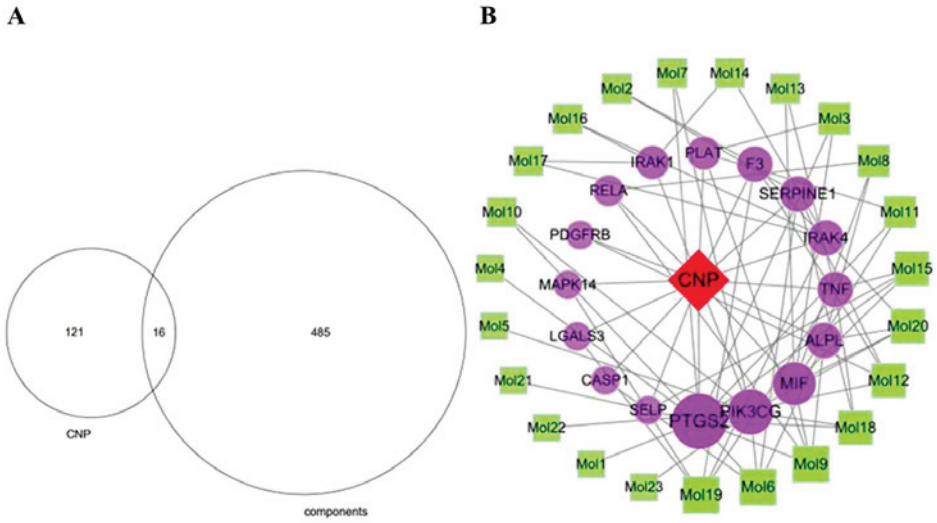

Figure 12. Venn diagram and network diagram of the chemical components and CNP targets. (A) Venn diagram of the chemical components and CNP targets. (B) Network diagram of CNP-components-targets. CNP, chronic nonbacterial prostatitis.

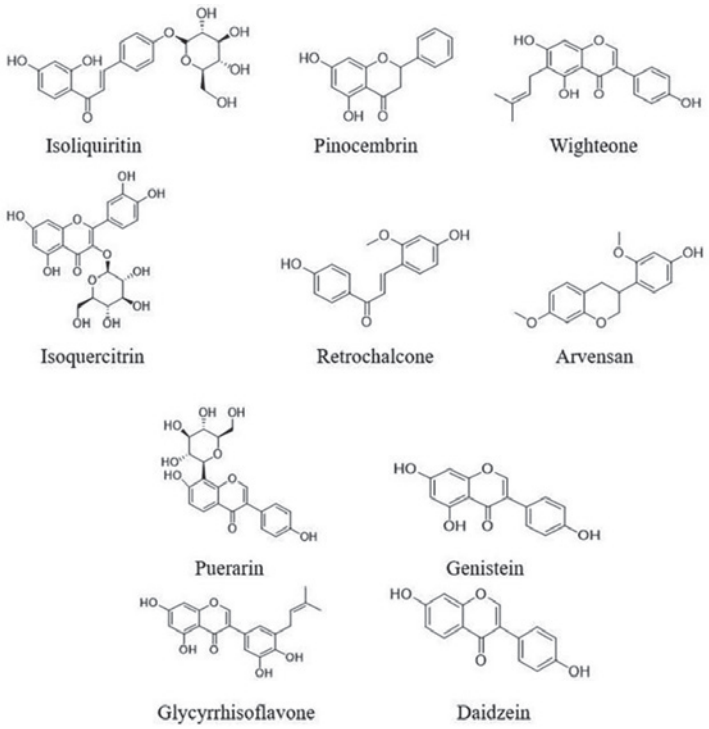

Figure 13. Chemical structures of the top 10 components based on the network diagram of the chronic nonbacterial prostatitis component targets.

CNP target prediction. A total of 137 potential CNP targets were screened in Genecards and OMIM using the term 'Chronic Nonbacterial Prostatitis'.

Construction of the component-CNP-target gene network. The 137 CNP targets were compared with the 501 component targets to obtain 16 common targets (Fig. 12A). The component-CNP-target network contained 40 nodes including one disease, 23 components, 16 genes and 76 edges (Fig. 12B). The green squares represent the chemical components, the purple circles represent the target genes, and the red diamond represents CNP. Importance is portrayed proportional to node size. The degree value of a node represents the number of other nodes connected to it in the network. Analysis of the nodes with large degree values screened using network topology indicated that nodes with relatively more chemical components or targets play pivotal roles in the entire network and may be key chemical components or targets. The top 10 components were CAS5041-81-6 (Isoliquiritin; 5 nodes), CAS480-39-7 (Pinocembrin; 5 nodes), CAS51225-30-0 (Wighteone; 5 nodes), CAS21637-25-2 (Isoquercitrin; 4 nodes), CAS34221-41-5 (Retrochalcone; 4 nodes), CAS63631-41-4 (Arvensan; 4 nodes), CAS3681-99-0 (Puerarin; 3 nodes), CAS446-72-0 (Genistein; 3 nodes), CAS116709-70-7 (Glycyrrhisoflavone; 3 nodes) and

Table III. Core active components and their topological properties.

No.	CAS	Name	Chemical formula	Degree	Type
1	5041-81-6	Isoliquiritin	$C_{21}H_{22}O_9$	5	Chalcone Oxide
2	480-39-7	Pinocembrin	$C_{15}H_{12}O_4$	5	Flavonone
3	51225-30-0	Wighteone	$C_{20}H_{18}O_5$	5	Prenylated Flavonoid
4	21637-25-2	Isoquercitrin	$C_{21}H_{20}O_{12}$	4	Flavonol Glycoside
5	34221-41-5	Retrochalcone	$C_{16}H_{14}O_4$	4	Chalcone
6	63631-41-4	Arvensan	$C_{17}H_{18}O_4$	4	Benzopyrone
7	3681-99-0	Puerarin	$C_{21}H_{20}O_9$	4	Isoflavone Oxyglycoside
8	446-72-0	Genistein	$C_{15}H_{10}O_5$	3	Isoflavone
9	116709-70-7	Glycyrrhisoflavone	$C_{20}H_{18}O_6$	3	Prenylated Isoflavone
10	486-66-8	Daidzein	$C_{15}H_{10}O_4$	3	Isoflavone

CAS Chemical Abstracts Service accession number.

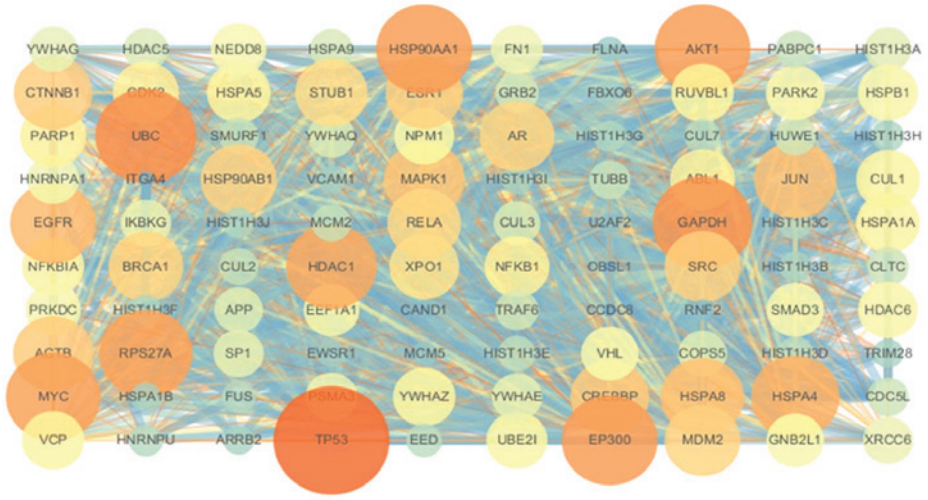

Figure 14. PPI network. The 100 core targets of the chemical components and chronic nonbacterial prostatitis were placed in the Search Tool for the Retrieval of Interacting Genes/Proteins to build the PPI network to filter important targets of the 100 core targets. PPI, Protein-Protein Interaction.

CAS486-66-8 (Daidzein; 3 nodes). Details of these components are shown in Table III and Fig. 13. The top three targets were PTGS2, PIK3CG and MIF, which interacted with 12, 8 and 7 chemical components, respectively.

Construction of the PPI networks. A total of 100 core targets were screened using Cytoscape. The PPI network (Fig. 14) showed strong associations between the targets and the complex interlaced networks. The network contained 100 nodes, which were the core targets of the aerial part of *Glycyrrhiza uralensis* in CNP treatment. TP53, AKT1, EP300, EGFR, HDAC1 and MYC were the hub genes.

GO and KEGG enrichment analyses. GO enrichment was performed to identify the gene intersections. A total of 1,392 top-ranking biological process terms were selected, including the cytokine-mediated signaling pathway, response to growth factor, regulation of cellular response to stress, regulation of cell cycle process and apoptotic signaling pathway (Fig. 15A). The molecular function terms consisted of protein domain specific, ubiquitin protein ligase, transcription factor, kinase and cadherin binding, amongst others (Fig. 15B). Enrichment analysis of the cellular components (Fig. 15C) showed that the targets were the perinuclear cytoplasmic region, transferase complex, protein-DNA complex, focal adhesion and nuclear body, amongst others.

KEGG pathway enrichment was performed to cluster the major effects associated with CNP. The top 20 ranking pathways were screened out ($P<0.01$; Fig. 15D). The main pathways were involved in cancer, including prostate cancer, estrogen, PI3K-Akt and MAPK signaling. The genes involved in these pathways are shown in Table IV.

Construction of the chemical component-pathway-target network. As shown in Fig. 16, the network showed that the components connected to the core target genes were glycyrrhisoflavone, wighteone, luteolin, diosmetin, isoliquiritin, Kaempferol, Gancaonin I, Galangin and Retrochalcone. Hence, these compounds may play major roles in the aerial part of *Glycyrrhiza uralensis*. Details of these top 9 components

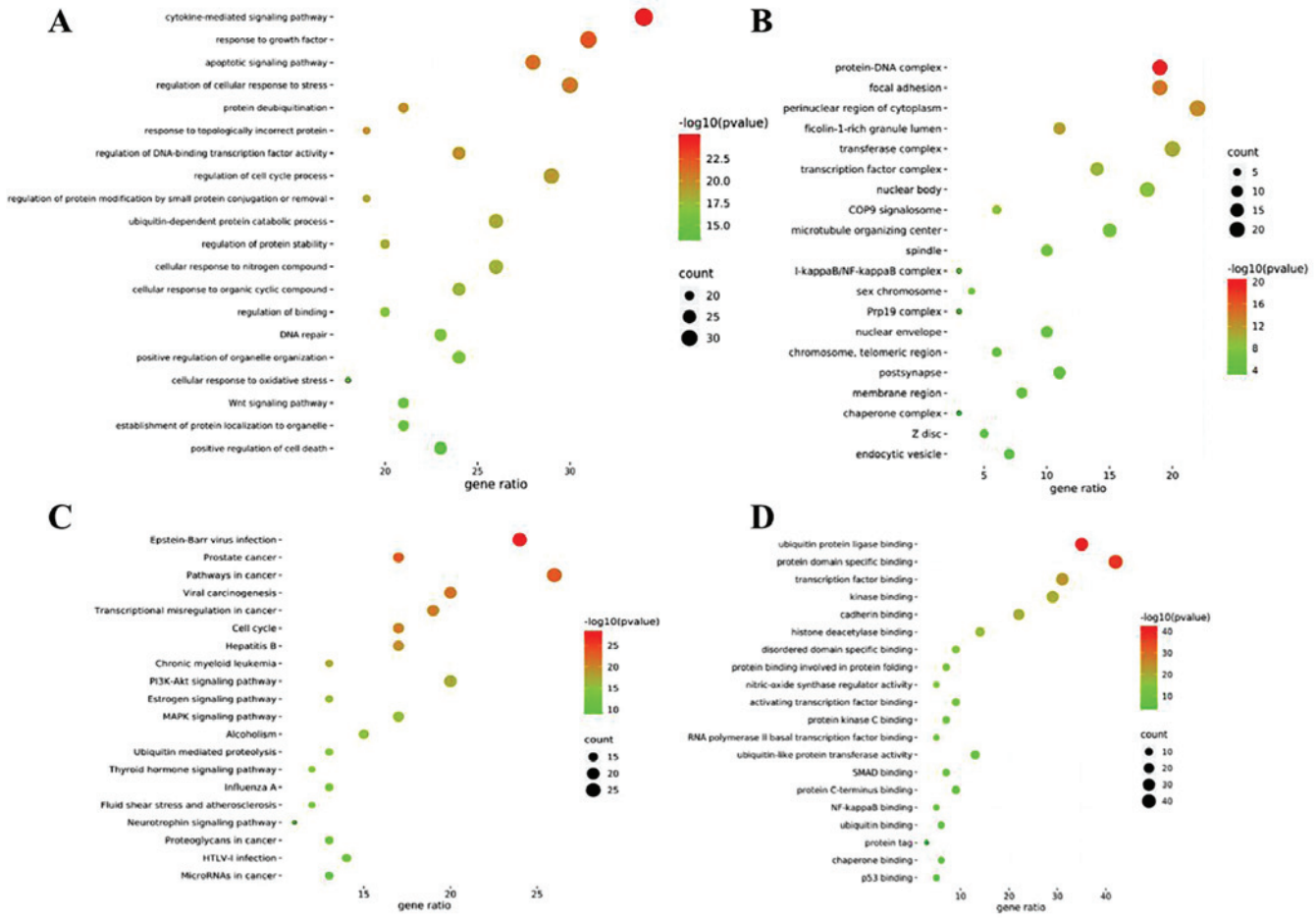

Figure 15. Top 20 results of GO functional and KEGG pathway enrichment analyses. (A) GO biological process; (B) molecular function; and (C) cell component. (D) KEGG pathway enrichment. GO, Gene Ontology; KEGG, Kyoto Encyclopedia of Genes and Genomes.

are shown in Table V and Fig. 17. Protein kinase-associated receptors (AKT1 and MAPK1), cyclin-dependent kinase 2, inflammation-associated receptors (RELA, NFKB1 and HDAC1), cancer-associated receptors (TP53), growth factor-associated receptors (EGFR), and hormone metabolism-associated estrogen receptor 1 (ESR1) were nodal proteins in the entire network, and were identified by measuring the pathway-component-target degree value.

Discussion

At present, the root of the licorice ground biomass accounts for a large proportion (approximately one-third) of the total licorice amount harvested. Annually, ~50,000 tons of licorice roots are produced; however, the ground part is not well utilized (1).

Dong *et al* (29) demonstrated that the total content of flavonoids found in licorice ground biomass is >4X that of the licorice root and rhizome. The majority of the flavonoids are isoflavone rhizones and dihydroflavonoids in the licorice root and rhizome, with no repetitive composition of Ural licorice rhizoid and root and rhizome (30). Flavonoids have various pharmacological activities, such as free radical antioxidant (31), anti-tumor (32), anti-viral (32), anti-inflammatory (33), anti-inflammatory and analgesic activity (34), cardio and cerebrovascular protective properties, as well as a liver-preserving effect (35). Hence the aerial part of licorice has notable clinical prospects. Siracusa *et al* (36) studied the anti-inflammatory activity of different extraction sites of licorice leaves and found the ethyl acetate extraction site to be the best. Fan (1) concluded that the main flavonoids in ethyl acetate extract of licorice include 21 isoflavones, 17 dihydroisoflavones (alcohol), 5 dihydroflavonoids, 4 orangones, 6 rosewood (alkene) and 4 Charketones. The primary anti-inflammatory active parts of flavonoids are the side and lipophilic components.

In the male reproductive system, there is a blood-testicular barrier and a blood-epididymal barrier, which protects the sperm, and the blood-prostate barrier also limits drug entry (37). Thus, the concentration of drugs in the prostate tissue is lower than that in the plasma, and hence the therapeutic effect is poor, whereas substances with strong lipophilicity can easily penetrate the blood-prostate barrier. The above ground liposoluble substances of *Glycyrrhiza uralensis* showed a good effect on reducing the prostate index, but the underlaying mechanism remains to determined.

Combining pharmacological experiments and network pharmacology analysis, research found that the MCP-1 signal channel was involved in breast, prostate, colorectal, pancreatic, bladder and esophageal cancer. Lin *et al* (38)

Table IV. Primary pathway targets.

Pathway in	Primary targets
Cancer	ABL1, AKT1, AR, CDK2, CREBBP, EGFR, CTNNB1, EP300
Prostate cancer	CDK2, CREBBP, EP300, AKT1, EGFR, MAPK1
Viral carcinogenesis	CDK2, CREBBP, EP300, GRB2, JUN, MDM2, NFKBIA, MAPK1
Estrogen signaling	AKT1, EGFR, ESR1, GRB2, HSPA1A, HSPA1B, HSPA8, HSP90AA1
Thyroid hormone signaling	ACTB, AKT1, CREBBP, CTNNB1, EP300, ESR1, HDAC1
Epstein-Barr virus infection	AKT1, CDK2, CREBBP, EP300, HDAC1, HSPA1A, HSPA1B, HSPA8
PI3K-Akt signaling	AKT1, BRCA1, CDK2, EGFR, FN1, HSP90AA1, HSP90AB1
MAPK signaling	AKT1, ARRB2, EGFR, FLNA, GRB2, HSPA1, AHSPA1B, HSPA8

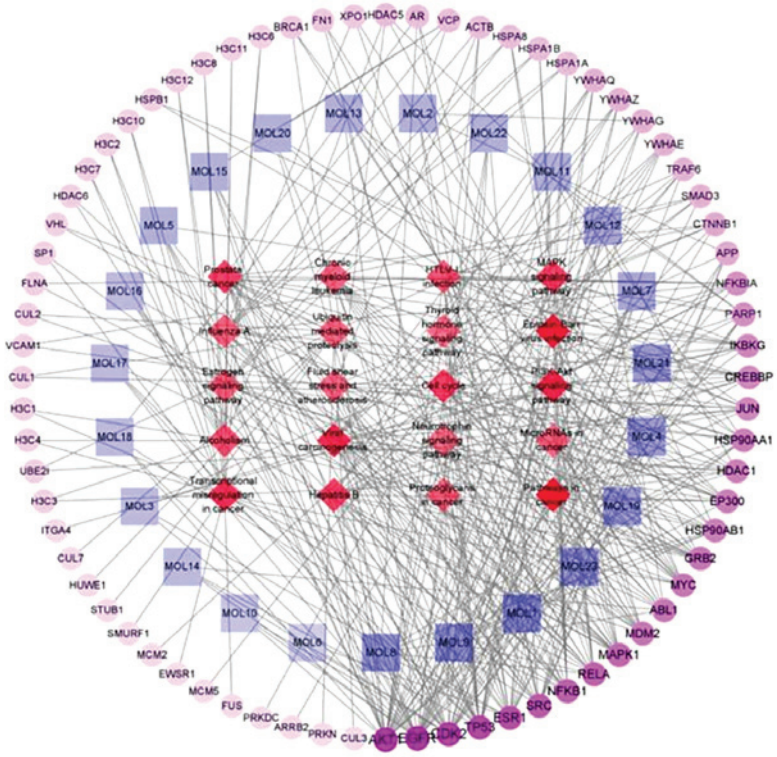

Figure 16. Pathway-component-target network diagram. This network, generated using Cytoscape, depicted the complex relationships amongst genes, components and pathways.

demonstrated that MCP-1 activates the PI3K/Akt signal channel by mediating mTORC1 activation, thus stimulating the proliferation and metastasis of prostate cell strains, such as PC3 and VCaP, which inhibits autophagy-mediated death of prostate cancer cells. Guyon *et al* (39) found that MCP-1 could also induce small gliocytes to produce TNF-α, which can promote the production of T lymphocytes, in-turn promoting the pathogenesis of inflammation and thus participating in the development of disease via induction of NF-κB. MAPK is an important transmitter of signals from the cell surface to the nucleus, and the p38-MAPK pathway is one of the best studied pathways in this family. Deng *et al* (40) found that parasitic extracts simultaneously achieved anti-inflammatory and anti-oxidative stress through the regulation of the MAPK and NF-kB pathways.

TNF-α plays an important role in the activation of multiple inflammatory factors and increases vascular permeability and accelerates the release and aggregation of various inflammatory factors, including prostaglandin-E2 (PGE-2) (41). Regulation of TNF-α is closely related to the expression of the NF-κB. Certain extracellular stimulatory signals activate NF-κB *in vivo*, thereby enhancing the transcription of the TNF-α gene and promoting TNF-α expression (42). TNF-α can then reactivate NF-κB via a positive feedback mechanism, which not only increases TNF-α secretion, but also induces the production and release of other pro-inflammatory cytokines, such as IL-1 and IL-8, resulting in a series of cascade responses leading to further amplification of the initial inflammatory signal (43).

PGE-2 is prevalent in tissues *in vivo*, and is one of the metabolites of arachidonic acid (AA), where COX-2

Table V. Core active components and their topological properties.

No.	CAS	Name	Chemical formula	Degree	Type
1	116709-70-7	Glycyrrhisoflavone	$C_{20}H_{18}O_6$	8	Prenylated Isoflavone
2	51225-30-0	Wighteone	$C_{20}H_{18}O_5$	8	Prenylated Flavonoid
3	491-70-3	Luteolin	$C_{15}H_{10}O_6$	8	Flavone
4	520-34-3	Diosmetin	$C_{16}H_{12}O_6$	7	Flavone
5	5041-81-6	Isoliquiritin	$C_{21}H_{22}O_9$	7	Chalcone Oxide
6	520-18-3	Kaempferol	$C_{15}H_{10}O_6$	7	Flavone
7	126716-36-7	Gancaonin I	$C_{21}H_{22}O_5$	7	Prenylated Flavonoid
8	548-83-4	Galangin	$C_{15}H_{10}O_5$	6	Flavonol
9	34221-41-5	Retrochalcone	$C_{16}H_{14}O_4$	6	Chalcone

CAS Chemical Abstracts Service accession number.

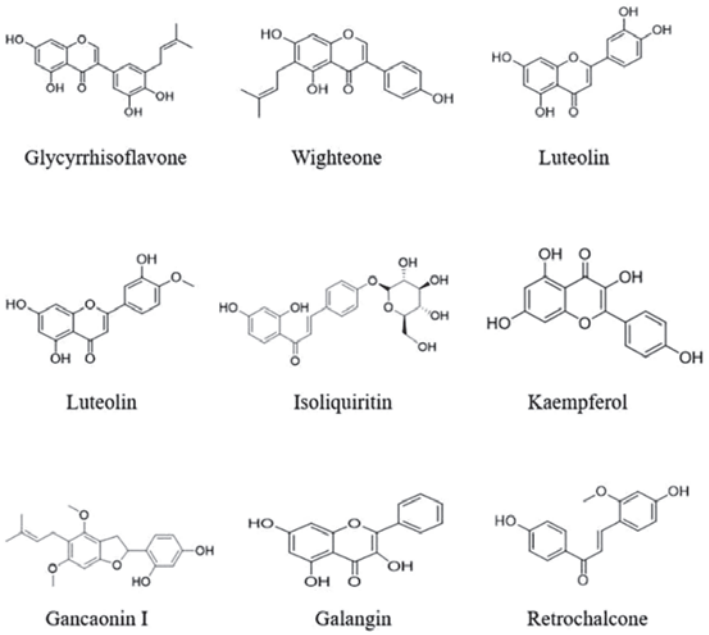

Figure 17. Chemical structures of the top nine active components of *Glycyrrhiza uralensis*.

transforms AA into multiple species by catalyzing epoxy oxygenation. Prostaglandin (PG) substances, which then serve a peroxidase function, convert PGG2 to PGH2, which under various synthases are converted to multiple peanut acid, such as PGE-2, which are finally passed downstream through different G protein receptors (44). Various studies have shown that PGE2 is an important inflammatory medium that can directly result in the increase in tissue vascular permeability and promote the secretion of inflammatory factors, such as IL-6 in relevant tissues (45). COX-2 is a rate-limiting enzyme for PGE-2 synthesis, and serves an important role in regulating the activity of PGE-2 (46).

NF-κB is a transcription factor that belongs to the Rel family, which is involved in regulating the transcription of genes involved in immunity and inflammation (47). The results of pharmacological experiments showed that water and alcohol may counter CNP by regulating the oxidative stress response, body immune response and hormones, and this appeared to more prominent with water group. Network pharmacological analysis showed that anthocyanins, Kaempferol, Retrochalcone, Glycyrrhisoflavone, arvensan and wighteone can regulate inflammation by regulating the proportion of hormones. Wighteone can regulate inflammation by managing inflammatory factors, and kaempferol can regulate inflammation by managing immunity.

Analysis of the pharmacological network showed that the aerial part of *Glycyrrhiza uralensis* reduced the inflammatory response in CNP via multiple mechanisms. The inflammatory response is attenuated by regulating inflammatory factor secretion. Abnormal inflammatory cytokine (such as TNF-α, IL-1, IL-2, IL-6, IL-8, IL-10, IL-1β, COX-2 and IFN-γ) levels have been reported in the semen and prostate fluid of patients with chronic prostatitis (48). Proinflammatory cytokines enhance inflammatory cell infiltration and adhesion to prostate gland epithelial cells, and stimulate abnormal cellular hypertrophy, dysregulate glandular secretion and promote

apoptosis (49). These factors are closely associated with inflammatory signaling pathways. Activated TNF-α binds to its receptors, TNFR1 and TNFR2, in the cell membrane and upregulates several genes in the MAPK pathway, which regulates NF-κB expression; the NF-κB signaling pathway is important in the inflammatory process (50). Fan *et al* (52) found that NF-κB was upregulated in patients with CNP and induced the secretion of various proinflammatory factors and aggravated inflammation. PI3K-AKT is upstream of the NF-κB signaling pathway. Activation of PI3K-AKT signaling can induce NF-κB, which in-turn induces inflammation. The majority of flavonoids exhibit an anti-inflammatory effect. The diagram of the chemical component-pathway-target network showed that wighteone is associated with NFKB1, and may reduce inflammation by regulating proinflammatory factor secretion.

RELA, which is associated with glycyrrhisoflavone and wighteone, is an inflammatory receptor. Glycyrrhisoflavone and wighteone can attenuate the inflammatory response by regulating the pathways associated with inflammation. Huang *et al* (53) reported that kaempferol significantly downregulated THP-1 in the MAPK pathway induced by lipopolysaccharides in a human monocytic leukemia cell line. Kaempferol suppressed inflammatory factors, such as macrophage-derived chemokine (MDC), IFN-induced protein-10 (IP-10) and IL-8. Panathur *et al* (54) found that repressing the transcription of multiple inflammation-related genes decreased the occurrence and impeded the progression of inflammatory responses. HDAC1 is a type III histone deacetylase, an important PPI target, and a part of the chemical component-pathway-target network, which downregulates several inflammation-related genes by deacetylating histones, NF-κB and activated protein 1. Hence, it regulates the occurrence and progression of the inflammatory response. Analysis of the chemical component-pathway-target network revealed that isoliquiritin and retrochalcone are associated with HDAC1, and may also attenuate inflammation by preventing the transcription of inflammation-related genes.

Zhuo *et al* (55) reported that oxidative stress is the primary cause of cancer and inflammation, amongst other diseases. In prostatitis, numerous inflammatory factors are released in response to local inflammatory reactions. In turn, excess free radicals are generated, peroxidation occurs, high levels of ROS form in the prostate microenvironment; thus, antioxidant enzymes, such as SOD, CAT and GSH-Px are inactivated, and MDA production increases. When cellular ROS and reactive nitrogen species (RNS) are produced faster than they are removed, they accumulate in large quantities and cause oxidative stress (56). Schaftoside inhibits the release of NO and various proinflammatory factors through the NF-κB, MAPKs and Nrf2-Keapl pathways; in this manner, it reduces the inflammatory response (57).

Of the top 20 pathways enriched in KEGG, six were associated with cancer. Prostatitis is closely related to cancer and studies have shown that prostate cancer is often accompanied by chronic inflammation (58). Popovics *et al* (59) found that chronic prostatitis and prostate cancer are associated with EGFR expression, whereas the analysis in the present study showed that EGFR was the primary target in the chemical component-pathway-target network. Herein, it was shown that 19 chemical components, including luteolin, isorhamnetin, galangin, glycyrrhisoflavone, wighteone, and retrochalcone were related to EFGR. These components may regulate inflammation through the cancer signaling pathway. IL-6 is associated with chronic inflammation in prostate cancer and regulates prostate cancer cell proliferation and apoptosis via the JAK, MAPK and PI3-K signaling pathways (60). Luteolin sensitizes cancer cells to cytotoxic drugs, regulates the secretion of inflammatory factors, and suppresses cell survival pathways, such as P13K and NF-κB.

Chen *et al* (61) showed that tumor-suppressing gene upregulation induces inflammatory cytokine expression. The PPI network showed that TP53 had a maximum degree value in inflamed prostate cells. In contrast, TP53 was present only at low levels in normal prostate cells. When cells are under stress, relative TP53 expression and activity increase and tumor cell production is inhibited (62). Chen *et al* (61) demonstrated that the ΔNp63 in the TP53 family regulates gene clusters associated with cellular proliferation, survival, adhesion and inflammation. ΔNp63 overexpression may upregulate target genes and inflammatory cytokines. Thus, cancer is closely associated with inflammation. The chemical component-pathway-target network demonstrated that puerarin is associated with TP53, and may attenuate inflammation by preventing TP53 upregulation and regulating inflammatory factor expression.

Normal prostate growth and development is closely associated with the levels and ratios of testosterone, estradiol (E2) and other sex hormones. Studies have reported that endogenous estrogen induces chronic prostate inflammation and precancerous lesions in mice. The imbalance in the sex hormone ratio that occurs in aging men may promote prostate epithelial cell proliferation and differentiation, modulate vascularization, and trigger certain diseases. Isoflavones and coumarins are phytoestrogens that structurally resemble E2 (63). Zheng *et al* (64) reported that puerarin regulates estrogen receptor (ER)α encoded by estrogen receptor 1 (ESR1). Puerarin hinders uterine growth in combination with E2. Guo *et al* (65) showed that kaempferol is estrogen-like and activates the ER. The chemical component-pathway-target network analysis performed in the present study showed that isoliquiritin, pinocembrin, wighteone, retrochalcone, arvensan, puerarin, glycyrrhisoflavone, luteolin, diosmetin and kaempferol are associated with ESR1. Hence, these chemical components may reduce inflammation by regulating sex hormone ratios.

A previous study have demonstrated that prostatitis is closely associated with abnormal autoimmunity (66). In this disease state, IgG, IgA, IgM and secretory immunoglobulin A levels are significantly increased, whereas the levels of immunosuppressive factors are significantly decreased. Thus, prostatitis occurrence enhances immunity (67). The gene recombinant protein-UBC had a second-degree value in the PPI network and inhibited macrophage activation, the primary response when the mammalian innate immune system is induced. Macrophages secrete the proinflammatory factors TNF-α and IL-6. During inflammation, recombinant protein-UBC may suppress immune system activation by inhibiting macrophages (68). T lymphocytes are important components of cellular immunity, and $CD4^+$ are helper T lymphocytes (69). Lin *et al* (70) found that prostatitis

symptoms may be mitigated by reducing inflammatory $CD4^+$ infiltration. Mu *et al* (71) reported that kaempferol is a natural immunosuppressant that lowers the incidence of autoimmune diseases and organ transplant rejection caused by excessive T lymphocyte activation and proliferation.

The analyses herein suggested that the anti-CNP mechanism of the aerial part of *Glycyrrhiza uralensis* may involve repression of the inflammatory response via reduction of MDC, interferon-IP-10, IL-8 and other inflammatory factors in the MAPK, PI3-K and other signaling pathways affected by components such as wighteone and glycyrrhisoflavone. Inflammation may be attenuated by downregulating inflammation-related genes via components such as isoliquiritin and retrochalcone, and it may also be alleviated by decreasing ROS and RNS generation via components such as schaftoside and kaempferol. Chronic prostatitis is associated with EGFR and PDGFR expression, and therefore, prostate cancer. A total of 19 chemical constituents, including luteolin, isorhamnetin, galangin, glycyrrhisoflavone, wighteone and kaempferol are associated with growth factor-related receptors, such as EFGR. Chronic inflammation in prostate cancer may be attenuated by inhibiting cell survival pathways, such as P13K, NF-κB and XIAP, and enhancing cancer cell sensitivity to cytotoxic drugs, such as luteolin. Inflammation may be alleviated by modulating the sex hormone ratio and preventing prostate epithelial cell proliferation, differentiation and prostaglandin-promoted angiogenesis. Isoliquiritin, pinocembrin, wighteone, retrochalcone, arvensan, puerarin, glycyrrhisoflavone, luteolin, diosmetin and kaempferol are associated with the estrogen receptor, ESR1 and may reduce inflammation by regulating the sex hormone ratio. Prostate inflammation is also alleviated by inhibiting immune enhancement caused by excessive T lymphocyte activation and proliferation via substances such as kaempferol.

The results of the present study showed that comparison of different extraction of *Glycyrrhiza uralensis*, the trend in the ability of water group to reduce prostate index was the most notable, and was better than that of Qianliekang. The liposoluble substances of the aerial part *Glycyrrhiza uralensis* can easily penetrate the blood-prostate barrier and play a role in inhibiting prostatic hyperplasia. In the comparison experiments of the activities of different extraction parts, water and alcohol extraction groups exhibited an anti-CNP role. The chemical components were analyzed, and water extraction and alcohol extraction were primarily composed of flavonoids and some saponins. It was preliminarily speculated that the components of the aerial part of *Glycyrrhiza uralensis* that played a role in inhibiting inflammatory factors was primarily the flavonoids. Water extraction and alcohol extraction showed a good inhibitory effect on the pathological changes of prostate tissue and the expression of inflammatory factors and fibrotic factors in CNP rats, but no difference was confirmed when compared with positive drugs. Amongst these, the effect of water extraction on reducing the infiltration of inflammatory factors was slightly stronger than that of alcohol extraction. Overall, the effect of water on the chronic prostatitis rats was significant, and the chemical components responsible were primarily the liposoluble flavonoids.

In conclusion, the aerial part of *Glycyrrhiza uralensis* exhibits anti-CNP properties, which is exerted in a multi-component, multi-target and multi-pathway manner. It reduced the production of proinflammatory factors, down-regulated inflammation-related genes, reduced the oxidative stress response, suppressed the cell survival pathway, modulated sex hormone ratios, impeded immune enhancement and decreased the occurrence of inflammation. The present study proposed and tested a novel method of exploring the anti-CNP components in the aerial part of *Glycyrrhiza uralensis* and their modes of action, and provided a theoretical reference for the development of innovative anti-CNP drugs.

Acknowledgements

Not applicable.

Funding

This study was supported by the Institute of Medicinal Plant Development, Chinese Academy of Medical Sciences, and Peking Union Medical College, Beijing (grant no. 100193) and the National Key R&D Program of China (grant no. 2018YFC1706500).

Availability of data and materials

The datasets used and/or analyzed during the present study are available from the corresponding author on reasonable request.

Authors' contributions

HL designed the study, performed the experiments, analyzed the data, performed the literature review and drafted the manuscript. LZ performed the experiments. GC conceived the study and performed the literature search. JC and WW assisted in the design of the study, and in the acquisition, analysis and interpretation of data. All the authors have read and approved the final manuscript.

Ethics approval and consent to participate

All rats were handled according to the National Guidelines for the Care and Use of Laboratory Animals, and all animal experiments were approved by the Animal Ethics Committee of the Chinese Academy of Medical Sciences and Institute of Medicinal Plant Development (approval no. SLXD-20200902021).

Patient consent for publication

Not applicable.

Competing interests

The authors declare that they have no competing interests.

References

1. Jiang L, Akram W, Luo B, Hu S, Faruque MO, Ahmad S, Yasin NA, Khan WU, Ahmad A, Shikov AN, *et al*: Metabolomic and pharmacologic insights of aerial and underground parts of *Glycyrrhiza uralensis* fisch. ex DC. for maximum utilization of medicinal resources. Front Pharmacol 12: 658670, 2021.

2. Guo ZJ and Ma CJ: An overview of studies on flavonoids in the aerial part of *Glycyrrhiza uralensis*. Aerosp Med 16: 62-64, 2005.
3. Li SD, Fu L, Lu Q and Qiu C: Study on the flavononoids in the leaves of *Glycyrrhiza uralensis* fisch. J Jilin Agric Univ 18: 35-37, 1996 (In Chinese).
4. Cui YR, Chen P, Liu JH, Liu T and Zheng QS: Structure-activity relationship of flavonoids from *Radix Glycyrrhiza*. Shizhen Guo Yi Guo Yao 21: 3041-3043, 2010 (In Chinese).
5. Bo YY, Zhang YH, Yang L and Cui J: Study on different extraction methods and antioxidant activities of total flavones from the aerial parts of *Glycyrrhiza uralensis*. J Tradit Chin Med 39: 145-151, 2020 (In Chinese).
6. Soheila JM, Jesus FC and Beatriz C: Anti-inflammatory effects of flavonoids. Food Chem 299: 125124, 2019.
7. Zhang L, Kang XF, Li LH, Cui J and Wang WQ: Analysis of flavonoids in the aerial parts of *Glycyrrhiza uralensis* by HPLC-MS. J Liaoning Univ Tradit Chin Med 20: 48-51, 2018.
8. Zhu YX and Xu NG: Clinical treatment of chronic nonbacterial prostatitis of kidney-yang deficiency type by acupuncture of Sanhuang points. Zhen Ci Yan Jiu 44: 443-445, 2019 (In Chinese).
9. Yuan B: Clinical observation of integrated traditional Chinese and western medicine on chronic nonbacterial prostatitis of damp-heat stagnation syndrome. Shanxi J Tradit Chin Med 36: 25-27, 2020 (In Chinese).
10. Zhang L, Zhao ZH, Yu BL and Cui J: Effect of the aerial parts of *Glycyrrhiza uralensis* on chronic prostatitis rats. Chin Tradit Pat Med 41: 1407-1410, 2019 (In Chinese).
11. Qiu ZK, Liu ZT, Pang JL, Wu HB, Liu X, Yang ZM, Li X and Chen JS: A network pharmacology study with molecular docking to investigate the possibility of licorice against posttraumatic stress disorder. Metab Brain Dis: Aug 21, 2021 (Epub ahead of print).
12. Liu J, Liu J, Tong X, Peng W, Wei S, Sun T, Wang Y, Zhang B and Li W: Network pharmacology prediction and molecular docking-based strategy to discover the potential pharmacological mechanism of Huai Hua San against ulcerative colitis. Drug Des Devel Ther 15: 3255-3276, 2021.
13. Chen XL, Tang C, Xiao QL, Pang ZH, Zhou DD, Xu J, Wang Q, Zhao YX and Zhu QY: Mechanism of Fei-Xian formula in the treatment of pulmonary fibrosis on the basis of network pharmacology analysis combined with molecular docking validation. Evid Based Complement Alternat Med 2021: 6658395, 2021.
14. Hu M, Zhong Y, Xiao W, Wang Y, Tang T, Wang S, Cui H, Li T and Luo J: Deciphering the therapeutic mechanisms of Wuzi Ershen decoction in treating oligoasthenozoospermia through the network pharmacology approach. Evid Based Complement Alternat Med 2021: 5591844, 2021.
15. Qi X, Xu H, Zhang P, Chen G, Chen Z, Fang C and Lin L: Investigating the mechanism of scutellariae barbata herba in the treatment of colorectal cancer by network pharmacology and molecular docking. Evid Based Complement Alternat Med 2021: 3905367, 2021.
16. Liu ZH and Sun XB: Network pharmacology: New opportunity for the modernization of traditional Chinese medicine. Yao Xue Xue Bao 47: 696-703, 2012 (In Chinese).
17. Ma SJ, Zhao MM, Chang MY, Wang RM, Yu Y and Zhang Y: Network pharmacology of astragalus in the treatment of chronic nephritis. World J Integr Tradit West Med 15: 1467-1472, 1479, 2020.
18. Cao Z, Sloper DT and Nakamura N: Identification of altered proteins in the plasma of rats with chronic prostatic inflammation induced by estradiol benzoate and sex hormones. ACS Omega 6: 14361-14370, 2021.
19. Zhang L, Zhao Z, Yu B, Cui J, Hou J and Wang W: Effect of the aerial part of *Glycyrrhiza uralensis* on rats with chronic prostatitis. Chin Tradit Pat Med 41: 1407-1410, 2019 (In Chinese).
20. Holt JD, Garrett WA, McCurry TK and Teichman JM: Common questions about chronic prostatitis. Am Fam Physician 93: 290-296, 2016.
21. Yang C, Yao J and Chen T: The effect of Qianliekang tablets on the clinical efficacy, immune function, and inflammatory factor levels in the prostatic fluid of elderly chronic prostatitis patients. Am J Transl Res 13: 7363-7369, 2021.
22. Zeng H, He Y, Yu Y, Zhang J, Zeng X, Gong F, Liu Q and Yang B: Resveratrol improves prostate fibrosis during progression of urinary dysfunction in chronic prostatitis by mast cell suppression. Mol Med Rep 17: 918-924, 2018.
23. Shannon P, Markiel A, Ozier O, Baliga NS, Wang JT, Ramage D, Amin N, Schwikowski B and Ideker T: Cytoscape: A software environment for integrated models of biomolecular interaction networks. Genome Res 13: 2498-2504, 2003.
24. Fan Y, Liu W, Jin Y, Hou X, Zhang X, Pan H, Lu H and Guo X: Integrated molecular docking with network pharmacology to reveal the molecular mechanism of simiao powder in the treatment of acute gouty arthritis. Evid Based Complement Alternat Med 2021: 5570968, 2021.
25. Ashburner M, Ball CA, Blake JA, Botstein D, Butler H, Cherry JM, Davis AP, Dolinski K, Dwight SS, Eppig JT, *et al*: Gene ontology: Tool for the unification of biology. The gene ontology consortium. Nat Genet 25: 25-29, 2000.
26. The Gene Ontology Consortium: The gene ontology resource: 20 years and still GOing strong. Nucleic Acids Res 47 (D1): D330-D338, 2019.
27. Kanehisa M: Post-genome informatics. 1st edition. Oxford University Press, Oxford, 2000.
28. Li HL, Kang XF, Hou JL, Wang WQ and Wu HH: Study on purification process of total flavonoids in part of water extract from licorice. Journal of Liaoning University of TCM 18: 60-63, 2016.
29. Dong Y, Zhao M, Zhao T, Feng M, Chen H, Zhuang M and Lin L: Bioactive profiles, antioxidant activities, nitrite scavenging capacities and protective effects on H2O2-injured PC12 cells of *Glycyrrhiza glabra* L. leaf and root extracts. Molecules 19: 9101-9113, 2014.
30. Shakeri A, Akhtari J, Soheili V, Taghizadeh SF, Sahebkar A, Shaddel R and Asili J: Identification and biological activity of the volatile compounds of *Glycyrrhiza triphylla* Fisch. & C.A.Mey. Microb Pathog 109: 39-44, 2017.
31. Huang YT, Chi ZL, Wang SM, Wu HQ, Qin KM and Li WD: Research progress on licorice flavonoids and their antitumor activities. Chin J New Drugs 26: 1532-1537, 2017 (In Chinese).
32. Ma FX, Xue PF, Wang YY, Wang YN and Xue SY: Research progress of serum pharmacochemistry of traditional Chinese medicine. China Journal of Chinese Materia Medica 42: 1265-1270, 2017.
33. Lu T, Yang J, Gao X, Chen P, Du F, Sun Y, Wang F, Xu F, Shang H, Huang Y, *et al*: Plasma and urinary tanshinol from *Salvia miltiorrhiza* (Danshen) can be used as pharmacokinetic markers for cardiotonic pills, a cardiovascular herbal medicine. Drug Metab Dispos 36: 1578-1586, 2008.
34. Cheng T, Sheng T, Yi Y, Zhang T and Han H: Metabolism profiles of icariin in rats using ultra-high performance liquid chromatography coupled with quadrupole time-of-flight tandem mass spectrometry and in vitro enzymatic study. J Chromatogr B Analyt Technol Biomed Life Sci 1033-1034: 353-360, 2016.
35. Li HL, Kang XF, Hou JL, Wang WQ and Wu HH: Purification of total flavonoids of water extract from the aerial part of licorice. J Liaoning Univ Tradit Chin Med 18: 60-63, 2016 (In Chinese).
36. Siracusa L, Saija A, Cristani M, Cimino F, D'Arrigo M, Trombetta D, Rao F and Ruberto G: Phytocomplexes from liquorice (*Glycyrrhiza glabra* L.) leaves-chemical characterization and evaluation of their antioxidant, anti-genotoxic and anti-inflammatory activity. Fitoterapia 82: 546-556, 2011.
37. Urióstegui-Acosta M, Tello-Mora P, Solís-Heredia MJ, Ortega-Olvera JM, Piña-Guzmán B, Martín-Tapia D, González-Mariscal L and Quintanilla-Vega B: Methyl parathion causes genetic damage in sperm and disrupts the permeability of the blood-testis barrier by an oxidant mechanism in mice. Toxicology 438: 152463, 2020.
38. Lin TH, Liu HH, Tsai TH, Chen CC, Hsieh TF, Lee SS, Lee YJ, Chen WC and Tang CH: CCL2 increases αvβ3 integrin expression and subsequently promotes prostate cancer migration. Biochim Biophys Acta 1830: 4917-4927, 2013.
39. Guyon A, Skrzydelski D, De Giry I, Rovère C, Conductier G, Trocello JM, Daugé V, Kitabgi P, Rostène W, Nahon JL, *et al*: Long term exposure to the chemokine CCL2 activates the nigrostriatal dopamine system: A novel mechanism for the control of dopamine release. Neuroscience 162: 1072-1080, 2009.
40. Deng JS, Chi CS, Huang SS, Shie PH, Lin TH and Huang GJ: Antioxidant, analgesic, and anti-inflammatory activities of the ethanolic extracts of *Taxillus liquidambaricola*. J Ethnopharmacol 137: 1161-1171, 2011.
41. Haas S and Straub RH: Disruption of rhythms of molecular clocks in primary synovial fibroblasts of patients with osteoarthritis and rheumatoid arthritis, role of IL-1β/TNF. Arthritis Res Ther 14: R122, 2012.
42. Jing SH, Gao X, Yu B and Qiao H: Raf kinase inhibitor protein (RKIP) inhibits tumor necrosis factor-α (TNF-α) induced adhesion molecules expression in vascular smooth muscle bells by suppressing (nuclear transcription factor-κB (NF-kappaB) pathway. Med Sci Monit 23: 4789-4797, 2017.

43. Shindo S, Kumagai T, Shirawachi S, Takeda K and Shiba H: Semaphorin3A released from human dental pulp cells inhibits the increase in interleukin-6 and CXC chemokine ligand 10 production induced by tumor necrosis factor-α through suppression of nuclear factor-κB activation. Cell Biol Int 45: 238-244, 2021.
44. Armstrong JM, Boura AL, Hamberg M and Samuelsson B: A comparison of the vasodepressor effects of the cyclic effects of the cyclic endoperoxides PGG, and PGH2 with those of PGD2 and PGE2 in hypertensive and normotensive rats. Eur J Pharmacol 39: 251-258, 1976.
45. Kawada M, Inoue H, Ohba S, Yoshida J, Masuda T, Yamasaki M, Usami I, Sakamoto S, Abe H, Watanabe T, *et al*: Stromal cells positively and negatively modulate the growth of cancer cells: Stimulation via the PGE2-TNFα-IL-6 pathway and inhibition via secreted GAPDH-E-cadherin interaction. PLoS One 10: e119415, 2015.
46. Greenhough A, Wallam CA, Hicks DJ, Moorghen M, Williams AC and Paraskeva C: The proapoptotic BH3-only protein Bim is downregulated in a subset of colorectal cancers and is repressed by antiapoptotic COX-2/PGE_2 signalling in colorectal adenoma cells. Oncogene 29: 3398-3410, 2010.
47. Tian D, Ling S, Chen G, Li Y, Liu J, Ferid M and Bian K: Hypertensive nephropathy treatment by heart-protecting musk pill: a study of anti-inflammatory therapy for target organ damage of hypertension. Int J Gen Med 4: 131-139, 2011.
48. Wang X, Hai CX, Liang X, Yu SX, Zhang W and Li YL: The protective effects of acanthopanax senticosus harms aqueous extracts against oxidative stress: Role of Nrf2 and antioxidant enzymes. J Ethnopharmacol 127: 424-432, 2010.
49. Guo JJ and Zhou Y: Research progress in detection methods of chronic prostatitis. Med Recapit 21: 1268-1270, 2015.
50. Yang J: Changes and significance of NE, pH, IL-1β, TNF-α and PGE2 in EPS patients with type III prostatitis. J Clin Pathol Res 38: 2583-2588, 2018.
51. Scotece M, Conde J, Abella V, López V, Francisco V, Ruiz C, Campos V, Lago F, Gomez R, Pino J and Gualillo O: Oleocanthal inhibits catabolic and inflammatory mediators in LPS-activated human primary osteoarthritis (OA) chondrocytes through MAPKs/NF-κB pathways. Cell Physiol Biochem 49: 2414-2426, 2018.
52. Fan G, Jiang X, Wu X, Fordjour PA, Miao L, Zhang H, Zhu Y and Gao X: Anti-inflammatory activity of tanshinone IIA in LPS-stimulated RAW264.7 macrophages via miRNAs and TLR4-NF-κB pathway. Inflammation 39: 375-384, 2016.
53. Huang CH, Jan RL, Kuo CH, Chu YT, Wang WL, Lee MS, Chen HN and Hung CH: Natural flavone kaempferol suppresses chemokines expression in human monocyte THP-1 cells through MAPK pathways. J Food Sci 75: H254-H259, 2010.
54. Panathur N, Dalimba U, Koushik PV, Alvala M, Yogeeswari P, Sriram D and Kumar V: Identification and characterization of novel indole based small molecules as anticancer agents through SIRT1 inhibition. Eur J Med Chem 69: 125-138, 2013.
55. Zhuo MQ, Luo Z, Xu YH, Li DD, Pan YX, and Wu K: Functional analysis of promoters from three subtypes of the PI3K family and their roles in the regulation of lipid metabolism by insulin in yellow catfish *Pelteobagrus fulvidraco*. Int J Mol Sci 19: 265, 2018.
56. Zhang YW, Shao DY, Shi JL and Zhu J: A review on biological activities of kaempferol. Chin Bull Life Sci 29: 400-405, 2017.
57. Ďuračková Z: Some current insights into oxidetive stress. Physiol Res 59: 459-469, 2010.
58. Porcaro AB, Tafuri A, Novella G, Sebben M, Mariotto A, Inverardi D, Corsi P, Processali T, Pirozzi M, Amigoni N, *et al*: Inverse association of prostatic chronic inflammation among prostate cancer tumor grade groups: Retrospective study of 738 consecutive cases elected to a first random biopsy set. Urol Int 100: 456-462, 2018.
59. Popovics P, Cai R, Sha W, Rick FG and Schally AV: Growth hormone-releasing hormone antagonists reduce prostatic enlargement and inflammation in carrageenan-induced chronic prostatitis. Prostate 78: 970-980, 2018.
60. Nguyen DP, Li J and Tewari AK: Inflammation and prostate cancer: The role of interleukin 6 (IL-6). BJU Int 113: 986-992, 2014.
61. Chen Z, Zhang JL and Yang XP: The research progression of tumor suppressor TP53 and the new family members TP63 and TP73. J Inner Mongolia Med Univ 35: 57-62, 2013.
62. Ma ZM, Tian YJ, Wang ZP and Zhai ZX: Updated roles of SIRT1 in prostate diseases. Zhonghua Nan Ke Xue 22: 356-360, 2016 (In Chinese).
63. Ma J, Liu Y, Sun LN and Liu C: Clinical observation of serum testosterone and estradiol in patients with prostatitis and healthy people. Chin J Hum Sexuality 26: 25-26, 2017 (In Chinese).
64. Zheng GL, Zhang XY, Zheng JW, Meng QC and Zheng DS: Estrogen-like activity of total isoflavones of puerarin and puerarin. J Chin Med Mater: 566-568, 2002 (In Chinese).
65. Guo AJ, Choi RC, Zheng KY, Chen VP, Dong TT, Wang ZT, Vollmer G, Lau DT and Tsim KW: Kaempferol as a flavonoid induces osteoblastic differentiation via estrogen receptor signaling. Chin Med 7: 10, 2012.
66. Zhou XH, Han L, Zhou ZH, Liu ZD, Yang JX, Lv YW and You CL: Morphological and molecular biological peculiarities of the experimental automimune prostatitis rat model. Zhonghua Nan Ke Xue 11: 290-295, 2005 (In Chinese).
67. John H, Maake C, Barghorn A, Zbinden R, Hauri D and Joller-Jemelka HI: Immunological alterations in the ejaculate of chronic prostatitis patients: clues for autoimmunity. Andrologia 35: 294-299, 2003.
68. Zong A, Cao H and Wang F: Anticancer polysaccharides from natural resources: A review of recent research. Carbohydr Polym 90: 1395-1410, 2012.
69. Wei C, Liu C and Wang H: Effects of suplatast tosilate on CD4+ T cells and IL-6 in prostate tissue of rat model with chronic bacterial prostatitis. Chin J Androl 23: 10-13, 2009.
70. Lin SJ, Chou FJ, Lin CY, Chang HC, Yeh S and Chang C: New therapy with ASC-J9® to suppress the prostatitis via altering the cytokine CCL2 signals. Oncotarget 7: 66769-66775, 2016.
71. Mu JJ, Zeng YY, Huang XY, Zhao XH and Song B: Effects of Kaempferol on activation, proliferation and cell cycle of mouse T lymphocytes in vitro. Xi Bao Yu Fen Zi Mian Yi Xue Za Zhi 25: 1106-1108, 2009 (In Chinese).
72. Tang L, Gao XH, Zhao B, Luo JR, Shi XY, Ge R, Ban SR and Li QS: Design and synthesis of new disubstituted benzoxazolone derivatives that act as iNOS inhibitors with potent anti-inflammatory activity against LPS-induced acute lung injury. (ALI). Bioorg Med Chem 28: 115733, 2020.
73. Takahashi M, Khan MSI, Makino R, Cline MA and Tachibana T: Role of nitric oxide on zymosan-induced inhibition of crop emptying in chicks. Comp Biochem Physiol A Mol Integr Physiol 261: 111057, 2021.
74. Costales MG, Alam MS, Cavanaugh C and Williams KM: Extracellular adenosine produced by ecto-5'-nucleotidase (CD73) regulates macrophage pro-inflammatory responses, nitric oxide production, and favors Salmonella persistence. Nitric Oxide 72: 7-15, 2018.
75. Scailteux LM, Capelle V, Balusson F, Oger E, Vincendeau S, Mathieu R and Chapron A: Changes in prostate cancer screening practice by blood PSA testing between 2011 and 2017, a French population-based study. Curr Med Res Opin 37: 1435-1441, 2021.
76. Huang BX, Su HC and Sun FK: Compound ciprofloxacin suppository combined with ningbitai and yunnan baiyao for histological prostatitis with PSA elevation. Zhonghua Nan Ke Xue 18: 986-990, 2012 (In Chinese).
77. Brkljača BN, Gotić J, Šuran J, Brozić D, Klobučar K, Bojanić K and Vrbanac Z: Effect of prolonged submaximal exercise on serum oxidative stress biomarkers (d-ROMs, MDA, BAP) and oxidative stress index in endurance horses. BMC Vet Res 14: 216, 2018.